Materials Advances

Accepted Manuscript

This article can be cited before page numbers have been issued, to do this please use: E. Khalaf Shokr, S. S. Enaili, M. Samir, S. Elkot and A. Mohamed Mohamed Elsaghier, *Mater. Adv.*, 2026, DOI: 10.1039/D6MA00174B.

View Article Online
DOI: 10.1039/D6MA00174B

Optoelectronic characterization and thermoelectric figure of merit optimization of newly Spirothiadiazole- thienothiophene-based Macroheterocyclic compounds

E. Kh. Shokr[1], Souhaila S. Enaili[2], Moumen S. Kamel[3], Sh.A. Elkot[1], Ahmed M. El-Saghier[3]

[1]Physics Department, Faculty of Science, Sohag University, Sohag, 82524, Egypt
[2]Pharmaceutical Chemistry Department, Faculty of Pharmacy, University of Zawia, Al Zawia 16418, Libya
[3]Chemistry Department, Faculty of Science, Sohag University, Sohag 82524, Egypt

Abstract

This work is concerned with the synthesis of some novel organic compounds, examining their optoelectronic characteristics and experiencing their promises for thermoelectric applications. For this purpose, newly spirothiadiazole–thienothiophene-based macroheterocyclic compounds termed as Kz1–Kz3 have been successfully synthesized. The compound syntheses have been performed by a green approach, including a one-pot condensation of thienothiophene thiohydrazide with different ketones, resulting in good-yielding macrocyclic spiroheterocycles. By using FT-IR, NMR and elemental analyses, the compounds' structures have been confirmed. Thin film optical studies reveal strong absorption and high transparency in UV -Vis and NIR spectral ranges, respectively. Depending on the degree of conjugation, the energy gaps range from 2.99 to 3.26 eV with indirect allowed transitions. Dielectric and dispersion studies provided evidence of high refractive index and high polarizability confirming their potential as optoelectronic devices. The thermoelectric studies demonstrated that the samples are n-type semiconductors with negative Seebeck coefficients and temperature-dependent conductivities. The best thermoelectric performance among other compounds with a power factor (PF) of 366 $\mu W\ m^{-1}\ K^{-2}$ and a zT of 0.78 at 493 K after annealing at 200°C for 5 minutes was attained by Kz2 compound. The preliminary outcomes of this work clearly demonstrated the promise of spirothiadiazole–thienothiophene frameworks for use in next-generation flexible, eco-friendly thermoelectric and optoelectronic applications.

Keywords: Optoelectronic properties; Thermoelectric power, Thinothiophene; Macroheterocyclic

View Article Online
DOI: 10.1039/D6MA00174B

1. Introduction:

Great interest in green technology based on organic thermoelectric materials has arisen due to concerns about the exhaustion of traditional fossil fuel sources and the climate change impacts caused by these fuels.

Organic semiconductors have captivated researchers over the past few decades due to their extraordinary optical and electronic properties, solution processability, significant structural versatility, and opportunity as low-cost electronic devices capable of bending [1-5]. Among the numerous classes of conjugated organic molecules, heterocyclic compounds with fused thiophene units are notable for being tuneable and having high charge carrier mobility. In themselves, organic semiconductors are quite promising materials with a wide range of applications as organic light-emitting diodes (OLEDs) [6] organic photovoltaic cells (OPVs) [7] and organic field-effect transistors (OFETs) [8]. To this family of conjugated organic molecules, thienothiophene derivatives are similarly attractive building blocks for research, considering their extended conjugation and desirable electronic characteristics.

Fused-ring compounds condensed by two thiophene units are referred to as thienothiophenes. They feature a common bond of two thiophene units, and their fused structure allows them to maintain a planar and π-conjugated mode. Planarity is a requirement to allow the compounds to attain efficient intermolecular stacking and charge carriers to transport efficiently [9, 10]. The rigid and planar backbone of thienothiophenes will minimize torsional disorder while allowing improved thin film crystallinity and allowing forces for efficient π-π interactions – both properties that are preferable for optoelectronic devices [11-13]. The excellent application of substituted functional groups at various positions is attractive for tailored material properties that tune electronic conditions.

In recent years, attention has been placed on synthesizing new derivatives of thienothiophenes with multiple substituents to modify energy levels, band gaps and solubility of thienothiophenes [10, 13, 14]. These substituents have comprised electron-donating groups (EDGs) and electron-withdrawing groups (EWGs) to modify the electron-donating ability of thienothiophenes at the frontier molecular orbitals for fine-controlling absorption and emission properties as well as the ionization potentials and electron affinities [14-17]. This degree of molecular engineering can be important after synthesis of thienothiophenes to consider compatibility with the device architecture or simply the other functional layers.

View Article Online
DOI: 10.1039/D6MA00174B

In addition to their optical properties, the electrical properties of thienothiophenes-based materials are equally important for the incorporation of these materials into electronic devices. Charge carrier mobilities, conductivities, and stabilities indicate the usefulness of these materials as the active layers in OFETs and other devices [18-20]. There are excess design choices to enhance charge transport properties by increasing ordered molecular arrangements and decreasing trap densities, such as increasing backbone planarity, side-chain engineering to promote molecular alignment or utilizing donor–acceptor systems to enhance interactions between ordered molecules [21]. Moreover, the thieno[3,2-b] thiophene motif has often been touted as the one on account of its high level of conjugation and natural planeness, the thieno[2,3-b] thiophene motif provides an anti-delocalized electronic topology, wherein the spatial arrangement of sulfur atoms and fusion of rings explicitly puts a limit on delocalization. This controllable conjugation has been shown to be central in the control of optical band gaps, carrier densities and thermoelectric responsiveness in small-molecule organic semiconductors.

Thermoelectric power in organic materials has emerged as a new area of research, mainly because of attractive characteristics, such as low thermal conductivity, mechanical flexibility, potential low cost, and large-area fabrication. In organic semiconductors and conductive polymers, the thermoelectric effect functions like the inorganic counterparts when charge carriers move according to a temperature gradient. However, the charge transport mechanism is often localized, and unlike inorganic materials, the inherent disorder in molecular structure and arrangement leads to different behavior typically resulting in a higher Seebeck coefficient even though electrical conductivity is usually less than inorganic substances. Optimization of the Seebeck coefficient, electrical conductivity, and thermal conductivity can be achieved by way of manipulating molecular structure, doping levels, and processing methods towards a high thermoelectric figure of merit (ZT).

Here, the current study attempts to interrogatively probe the role of limited conjugation, spiro connectivity, and molecular conformations in optoelectronic and thermoelectric thin films in the solid state. The choice of the spirothiadiazole moiety to provide a three dimensional non-planar structure, which discourages intermolecular aggregation in excess and decreases the lattice thermal conductivity, an undesirable property in thermoelectric systems. Three new spirothiadiazole-thieno [2,3-b] thiophene based macro-heterocyclic compounds (Kz1-Kz3) were made via an environmentally friendly process, and used as model systems and the investigation

View Article Online
DOI: 10.1039/D6MA00174B

of their optical, electrical, and thermoelectric characteristics. The validity of these compounds to be applied for thermoelectric generation has been experienced, and the related parameters have been optimized.

2. Experimental

2.1. Preparation of thin films

The resultant thin films were placed onto clean glass substrates via spin coating with 0.003 g of the synthesized chemical diluted in 10 ml of alcoholic solution. The thickness of the thin films (300 ± 15 nm) was measured by surface profilometer (FORM TALYSURF 50).

2.2. Materials & techniques

Using percolated dishes of silica gel G/UV-254 with a 0.25 mm thickness (Merck 60F254) and UV light (254 nm/365 nm) to allow visualization, thin layer chromatography (TLC) was used to monitor all reactions. All melting points were recorded using the uncorrected Kofler melting point instrument. IR spectra were analyzed using KBr pellets on an FT-IR spectrophotometer. ^{13}C NMR (DMSO-d_6) and ^{1}H NMR spectra were recorded at Sohag University at 400 MHz and 100 MHz, respectively. Information on chemical shift, integration, and multiplicity (singlet, doublet, triplet, and multiplet) is given for ^{1}H NMR data. For internal measurement, tetramethylsilane (TMS) was chosen as the standard, and its chemical shifts (δ) were reported in parts per million (ppm). Internal standards for ^{13}C NMR were either DMSO (= 39.51 ppm) or TMS (= 0 ppm). The elemental analyses were performed using a Perkin-Elmer CHN analyzer model.

The absorbance, transmission, and reflection spectra were measured at normal incidence in the 200-2500 nm wavelength range using a computer-programmed double-beam spectrophotometer model Jasco 570 with reflectivity attachment model ISN 470 (Japan). VTC-50A spin coating has been employed to deposit thin coatings. Iodine doping was conducted under room temperature in a closed glass chamber whereby the thin films were sealed under saturated iodine vapor at a constant distance of approximately 5cm over 5min.The D.C. electrical resistance of the present films was determined using the two-probe approach. These measurements were taken using a multimeter (model number HP HEWLTTPACKARD 34401). A Silver paste electrode with a part spacing of 3 mm for the film was used. To regulate the

View Article Online
DOI: 10.1039/D6MA00174B

sample temperature throughout the 430-520 K range, the films were put in a software tube centre. The annealing process has been done by using a LINDBERG digital furnace.

Seebeck coefficient measurements were carried out in the conventional manner at a constant temperature difference ($\Delta T \sim 4$ degree) between the two ends of the film. The temperature difference was determined by measuring separately the thermovoltages at the film ends by means of a Keithley 191 digital multimeter. The generated thermopower was measured by a Keithley 614 digital electrometer.

2.3. Synthesis of Thienothiophene thiohydrazide Kz

In round bottomed flask, hydrazinecarbothiohydrazide **i** (0.002 mol) in 3 ml acetic acid as a catalyst and 15 ml ethanol was added to 1,1'-(3,4-dimethyl-3a,6a-dihydrothieno[2,3-b]thiophene-2,5-diyl)bis(ethan-1-one) **ii** (0.001 mol), and the reaction mixture was stirred under reflux for about five hours to afford (1Z,1'Z)-((3,4-dimethyl thieno[2,3-b]thiophene-2,5-diyl)bis(ethan-1-yl-1-ylidene))bis(hydrazine).

2.4. Synthesis of Spirothiadiazole-thinothiophene-based Macroheterocyclic

Thienothiophen thiohydrazide **Kz** (0.001 mol) in 15 mL of ethanol was mixed with ketones **1a, b** (0.002 mol) or (0.001 mol) **1b**, and the reaction mixture was stirred under reflux for about three hours without any catalyst. The solid precipitate was filtered, washed with ethanol, and then left to dry.

5',5'''-(((1Z,1'Z)-(3,4-dimethylthieno[2,3-b]thiophene-2,5-diyl)bis(ethan-1-yl-1-yl idene))bis(hydrazin-1-yl-2-ylidene))bis(2H,3'H-spiro[acenaphthylene-1,2'-[1,3,4]thiadiazol]-2-one) (*Kz1*)

Orange solid, Yield (96%). M.p. 218–220 °C. FT-IR (KBr) *v*max cm^{-1}: 3415, 3237(2NH), 3003($CH_{-arom.}$), 2856($CH_{-aliph.}$), 1685 (C=O $_{amide}$, st), and 1615 ((-HC=N-, st). ^{1}H-NMR (DMSOd_6),δ ppm: 14.19 (s, 1H, $NH_{hydrazone}$), 11.49 (s, 1H, $NH_{thiadiazole}$)8.44-7.82 (m, 7H, $CH_{arom.}$); 3.44 (s,3H, CH_3 $_{hydrazone}$) 2.65 (s, 3H, CH_3 $_{thiophene}$);^{13}C-NMR (DMSO-*d6*),δ ppm:182.45(C=O), 168.01(C=N), 159.00(C=N), 140.80, 140.54, 140.12, 135.03, 133.55, 132.62, 129.39, 129.57, 128.26, 127.23, 127.67, 126.05, 120.47($13C_{arom.}$), 82.43(C_{spiro}), 20.64(CH_3 $_{hydrazone}$) and 10.45(CH_3 $_{thiophene}$) .;C.F.: $C_{38}H_{28}N_8O_2S_4$,M.W.: 756.94.Elemental Analysis: calc.C, C, 60.30; H, 3.73; N, 14.80; O, 4.23; S, 16.94; Found, C, 60.63; H, 3.92; N, 14.57; S, 16.60.

5',5'''-(((1Z,1'Z)-(3,4-dimethylthieno[2,3-b]thiophene-2,5-diyl)bis(ethan-1-yl-1-yli dene))bis(hydrazin-1-yl-2-ylidene))bis(3'H-spiro[indoline-3,2'-[1,3,4]thiadiazol]-2-one) (*Kz2*)

View Article Online
DOI: 10.1039/D6MA00174B

Orange solid, Yield (98%). M.p. 205–207 °C. FT-IR (KBr) *v*max cm^{-1}: 3413, 3316,3232(3NH), 3003($CH_{-arom.}$), 2814($CH_{-aliph.}$), 1733(C=O $_{isatin}$, st), 1697 (C=O $_{amide}$, st), and 1619 ((-HC=N-, st). ^{1}H-NMR (DMSOd_6),δ ppm: 14.23 (s, 1H, $NH_{hydrazone}$), 11.51 (s, 1H, $NH_{thiadiazole}$)7.60-7.40 (m, 5H, CH $_{arom.}$); 3.44 (s,3H, CH_3 $_{hydrazone}$) 2.68 (s, 3H, CH_3 $_{thiophene}$);^{13}C-NMR (DMSO-*d6*),δ ppm:175.63(C=O), 163.71(C=N), 158.47(C=N), 141.58, 139.36, 137.43, 131.53, 129.30, 162.97, 123.34, 120.35, 110.78($9C_{arom.}$), 80.67(C_{spiro}), 20.49 (CH_3 $_{hydrazone}$) and 10.94 (CH_3 $_{thiophene}$) .;C.F.: $C_{30}H_{26}N_{10}O_2S_4$,M.W.: 686.85. Elemental Analysis: calc.C, C, 52.46; H, 3.82; N, 20.39; O, 4.66; S, 18.67; Found, C, 52.23; H,3.70; N, 20.68; O, 4.33, S, 18.91.

2,2'-[(Disulfanediylbis(1H-benzo[d]imidazole-2,1-diyl))bis(naphthalene-1,1'-diyl)]bis(dithieno [3,2-b:2',3'-d]pyrrole) (*Kz3*)

Orange solid, Yield (91%). M.p. 198–200 °C. FT-IR (KBr) *v*max cm^{-1}: 3414, 3236(2NH), 3003($CH_{-arom.}$), 2925($CH_{-aliph.}$), and 1615 ((-HC=N-, st). ^{1}H-NMR (DMSOd_6),δ ppm: 14.21 (s, 1H, $NH_{hydrazone}$), 11.51 (s, 1H, $NH_{thiadiazole}$) 8.33-7.82 (m, 6H, CH $_{arom.}$); 3.40 (s,3H, CH_3 $_{hydrazone}$) 2.72 (s, 3H, CH_3 $_{thiophene}$);^{13}C-NMR (DMSO-d_6),δ ppm:158.47(C=N), 151.64(C=N), 141.68, 139.36, 137.43, 131.53, 129.30, 126.97, 126.39, 123.34, 120.35, 110.78($13C_{arom.}$), 80.67(C_{spiro}), 21.74(CH_3 $_{hydrazone}$) and 10.77 . (CH_3 $_{thiophene}$).; C.F.: $C_{26}H_{22}N_8S_4$, M.W.: 574.09. Elemental Analysis: calc.C, C, 54.33; H, 3.86; N, 19.50; S, 22.31; Found, C, 54.00; H,4.01; N, 19.20; S, 21.95.

3. Results and discussion:

3.1.Chemistry

In continuation of our work in the synthesis of novel spiroheterocycles [22-26], we prepared in a new series of spirothiadiazole-thinothiophene-based Macroheterocyclic derivatives containing a 1,3,4-thiadiazole moiety. The desired compounds were synthesized by stirring thenothiophene thiohydrazide 1 under reflux with ketones 1 a-c in ethanol under green condition to afford spirothiadiazole-thinothiophene-based Macro heterocyclic derivatives Kz1-Kz3 (Scheme1).

View Article Online
DOI: 10.1039/D6MA00174B

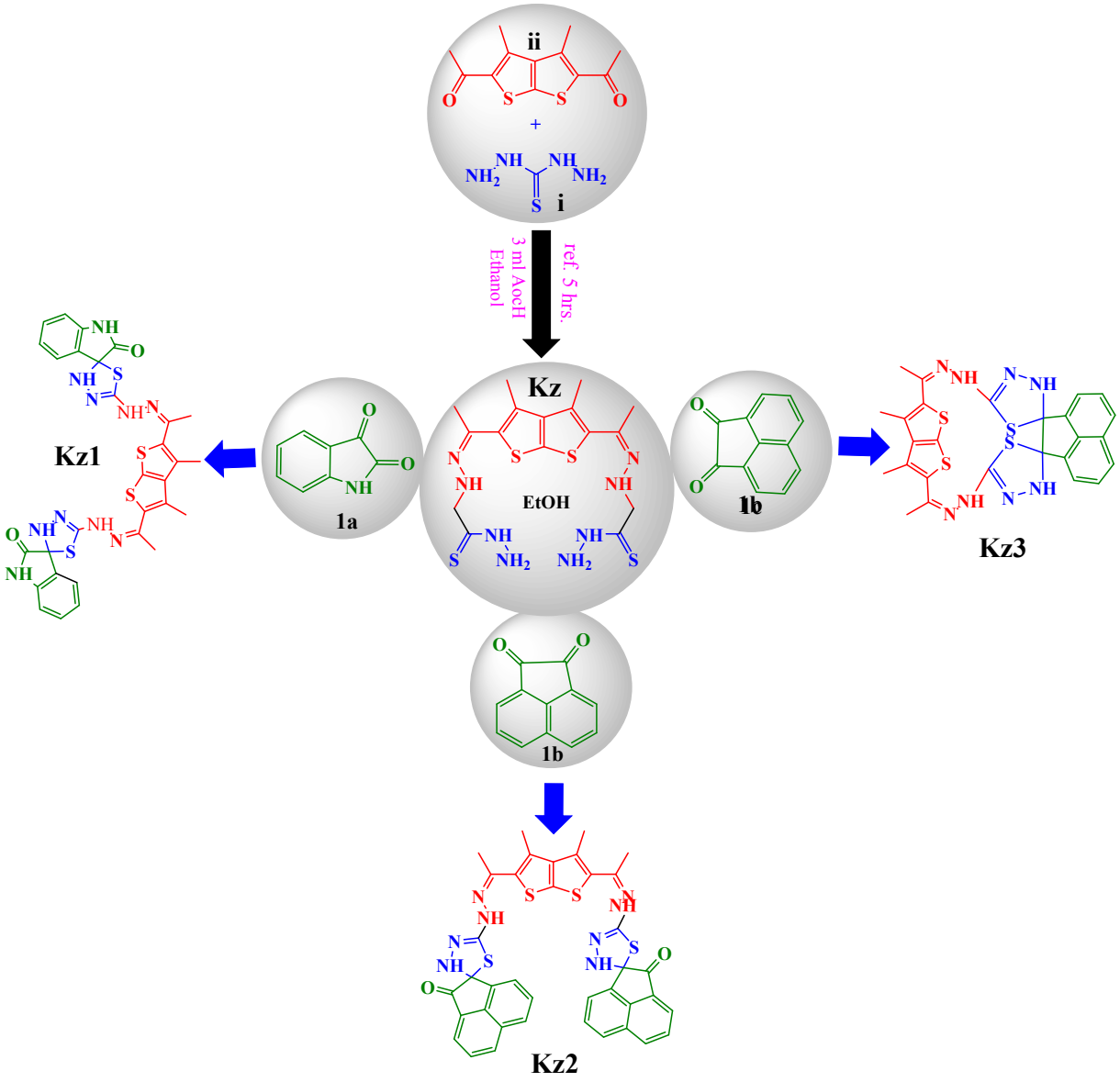

Scheme 1: Synthesis of spirothiadiazole-thinothiophene-based Macroheterocyclic derivatives Kz1-Kz3

3.2. Film microstructure

As shown by X – ray diffractograms (Fig. 1), Kz1, Kz2, and Kz3 are entirely amorphous microstructures [27] .

View Article Online
DOI: 10.1039/D6MA00174B

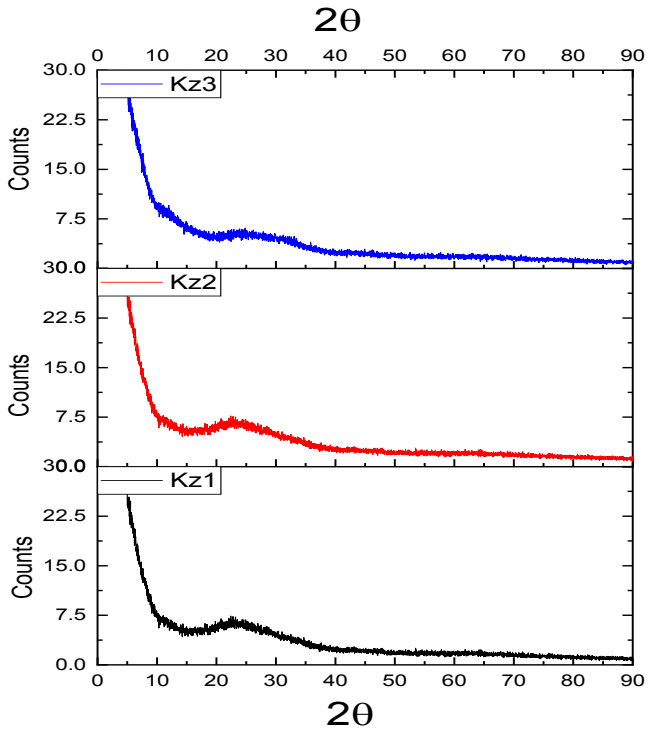

Fig. 1: XRD patterns of compounds Kz1, Kz2 and Kz3 thin films (300 $\pm$ 15 nm)

3.4. Optical properties investigation:

3.4.1. Optical analysis:

Fig. (2) illustrates the transmission and absorption spectra in the wavelength (λ) range of 300 – 2500 nm for present compound's thin films. Fig. (2a) reveals that the fundamental absorption edge for the compounds Kz1, Kz2, and Kz3 thin films exists in the wavelength of the $330 < \lambda < 380$ nm range (barely in the UV – Vis regions), which may be related to $\pi - \pi^*$ transition [28, 29]. Compound Kz1 shows high transmission nearly 65 - 70% at wavelength range of (500 to 2500 nm). However, compound Kz2, and Kz3 start with high transmission ($\sim$ 70%) then gradually decrease with increasing energy from NIR to $\sim$ UV spectral regions. This decrease in transmission can be attributed to the increase in absorption with hv increase as shown in Fig. 2b.

View Article Online
DOI: 10.1039/D6MA00174B

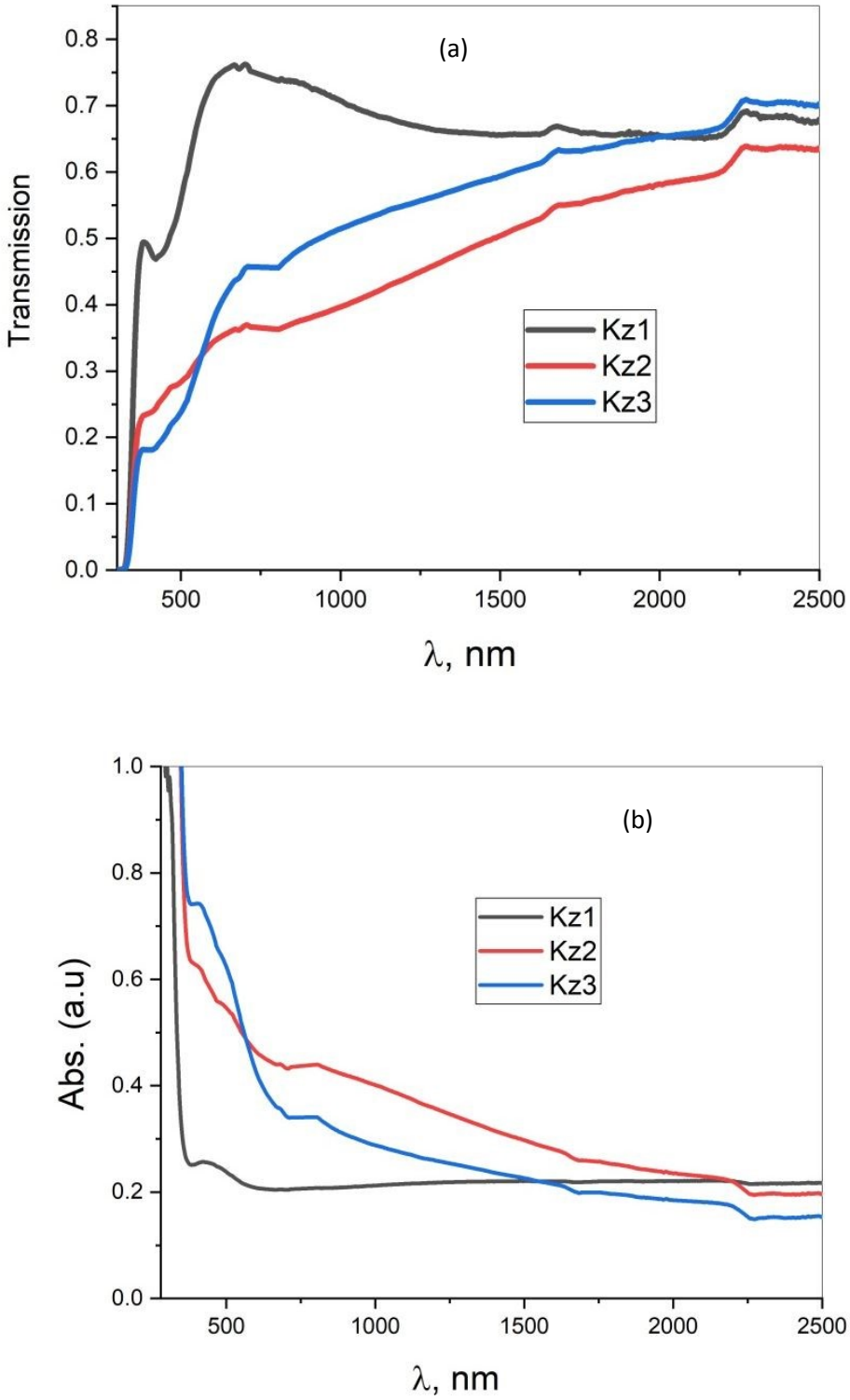

Fig. (2): Transmission (a) and absorption (b) spectra for compounds Kz1, Kz2 and Kz3 thin films.

View Article Online
DOI: 10.1039/D6MA00174B

Measured transmission and reflection spectra have been utilized to compute optical parameters including absorption coefficient α, refractive index n, and extinction coefficient k. When numerous reflections are neglected in a perfectly flat film and the substrate, the optical transmission T and subsequent α, n, and K can be obtained by the following equations [30, 31].

$$T = (1 - R)^2 \exp(-A) \quad (1)$$

$$\alpha = \frac{\text{Abs}}{\text{d}} = \frac{2.303}{\text{d}} \log\left[\frac{(1-\text{R})^2}{\text{T}}\right] \quad (2)$$

$$, \ \text{n} = \left(\frac{1+\text{R}}{1-\text{R}}\right) + \left[\left(\frac{1+\text{R}}{1-\text{R}}\right)^2 - (1 + \text{K}^2)\right]^{\frac{1}{2}} \quad (3)$$

$$\& \qquad \text{K} = \alpha\lambda/4\pi \quad (4)$$

, where d is the film thickness.

The spectral variations of refractive index n and extinction coefficient are important in various areas. The refractive index controls light refraction and transmission, while the coefficient of extinction determines light absorption. These optical constants are essential for design and adaptation in understanding optical devices, photonic components and even physical properties at a fundamental level [32, 33]. Table 1 shows the average values of the absorption coefficient (α_{500}), and refractive index (n_{500}), in the solar maximum wavelength (λ=500 nm) in comparison with the corresponding reported values of some organic materials.

The compound thin films (Kz1, Kz2, and Kz3) exhibit a high refractive index n around the UV region (Fig. 3a). A prominent peak appears at $473 \; to \; 605$ nm may be due to considerable absorption generated by electronic transitions around the band gap energy. The elevated refractive index over that area suggests that the material is significantly polarized. In addition, the refractive index in general shows normal dispersion behavior. Fig. (3.b) depicts the extinction coefficient of compounds Kz1, Kz2, and Kz3 thin films, revealing that the extinction coefficient is high in the UV region, then drops sharply near the fundamental absorption edge, and finally increases once again in the wavelength range of 500 to 2500 nm. Such behavior looks like and reflects the corresponding absorption spectrum (Fig. 2b).

View Article Online
DOI: 10.1039/D6MA00174B

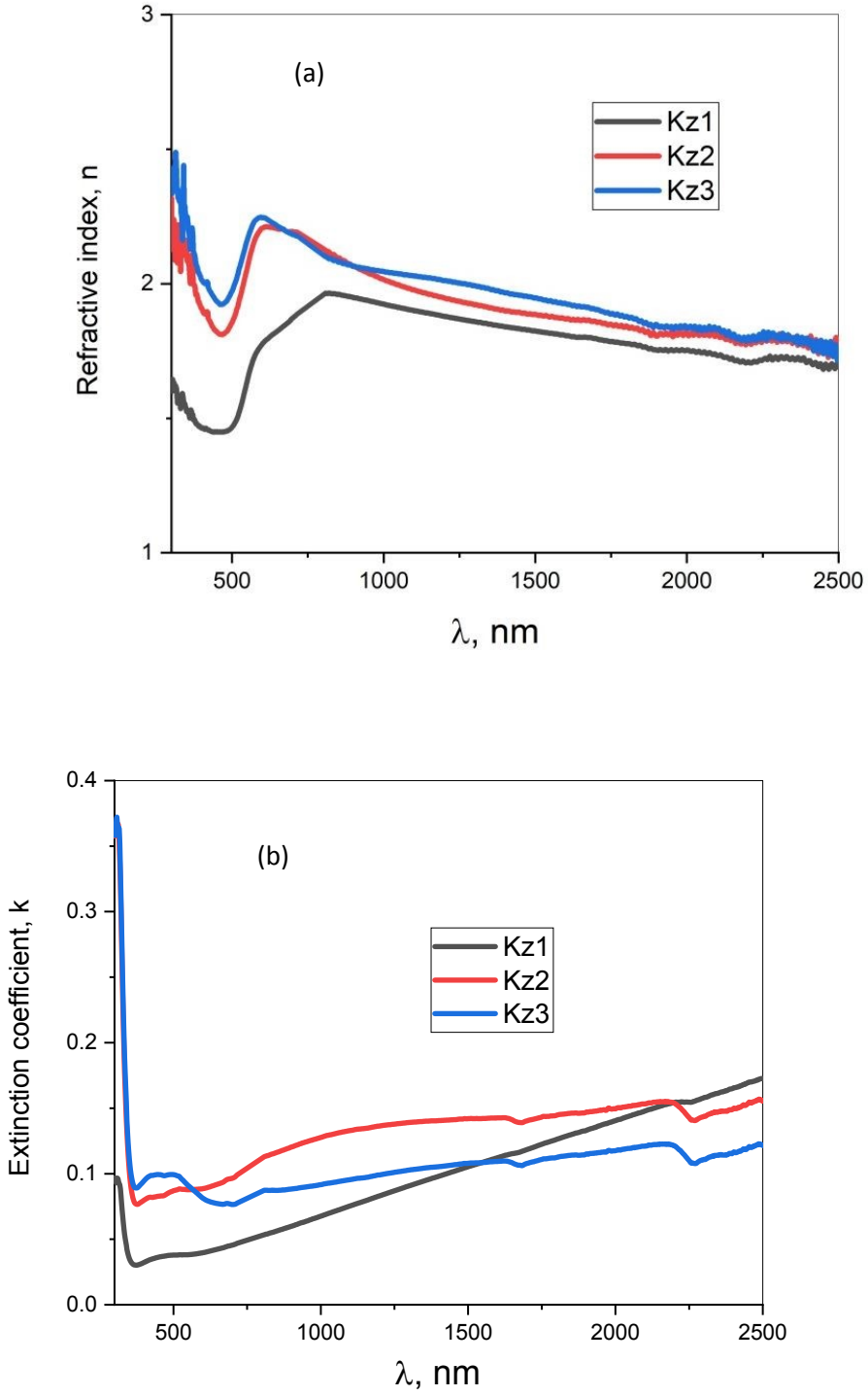

Fig. (3): Refractive index n (a) and extinction coefficient k (b) spectra for compounds Kz1, Kz2 and Kz3 thin films.

In the range of $1 < \alpha(cm^{-1}) < 10^4$, α varies exponentially with photon energy (hν), based on the density and tail width (E_u) of the localized states, which generally occur in the band

View Article Online
DOI: 10.1039/D6MA00174B

gap region of the amorphous non-metallic semiconductors, and verifies the following Urbach relation [34].

$$\alpha = \alpha_o \exp\left(\frac{h\nu}{E_u}\right) \quad (5)$$

In this equation, α_o is a constant, and E_u is the energy width of localized states. E_u values were computed using the slopes of the lnα vs. hν plots (Fig. 4) and documented in Table 1. The E_u values for compound Kz3 > Kz2 > Kkz1 thin films can correspond to the microstructure and/or π − conjugation number [4, 35, 36].

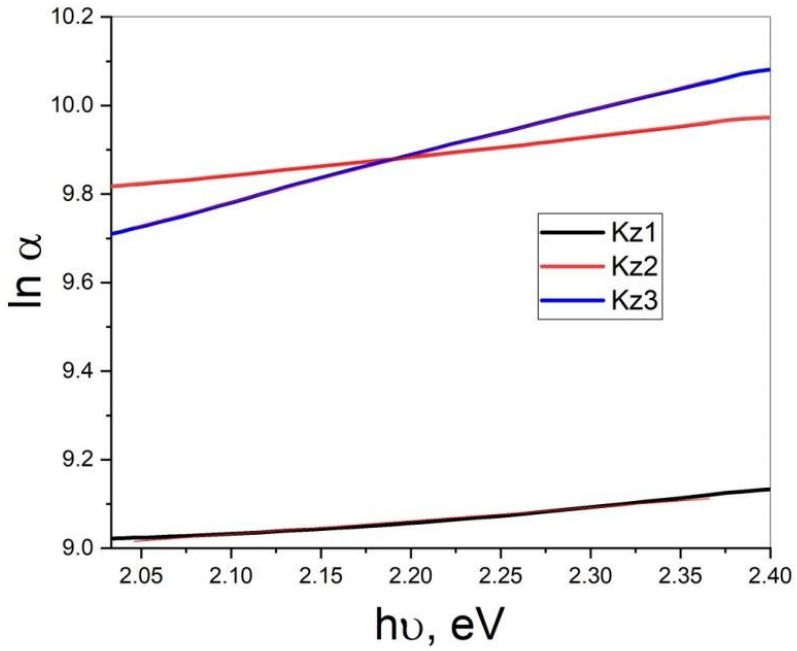

Fig.(3): plots lnα vs. hν for compounds Kz1, Kz2 and Kz3 thin films.

The penetration depth δ is a vital optical characteristic that indicates how far incident light could penetrate a substance before its intensity is noticeably reduced. It also relates to the absorption coefficient and heavily relies on the wavelength and physical structure of the substance. The penetration depth could be determined using the equation below:

$$\delta = \frac{\lambda}{4\pi k} = \frac{1}{\alpha'}, cm$$

Fig. (5) demonstrates that compound kz3 has a high penetration depth in the wavelength region of 1500 to 2500 nm, which can be attributed to its low extinction coefficient, making it a

View Article Online
DOI: 10.1039/D6MA00174B

potential material for IR sensors. Compound kz1 exhibits a high extinction coefficient; therefore, its penetration depth is high in the 300–1500 nm wavelength range, making it appropriate for surface-sensitive device uses.

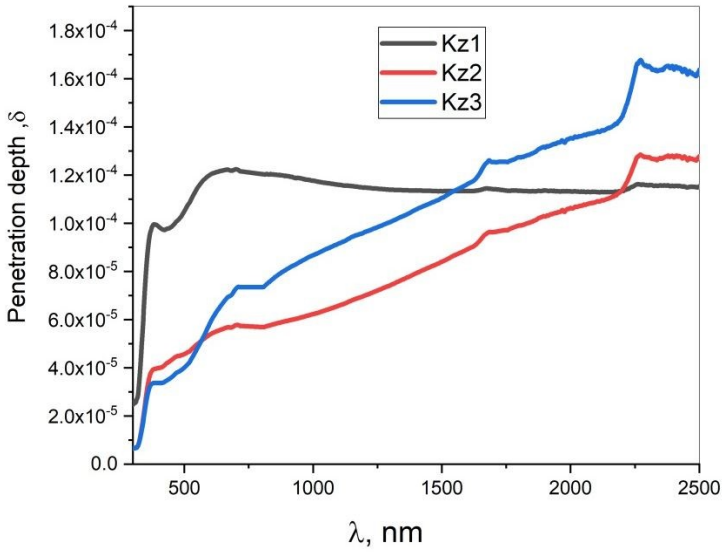

Fig. (5): Light wavelength dependence of penetration depth for compounds Kz1, Kz2 and Kz3 thin films.

The Moss criterion [37] can be used to estimate absorption transitions and band gap energies. The band gap value E_g is calculated by determining the value of λ that occurs when the slope of the absorption coefficient is a maximum near the absorption edge [38-41]. The absorption coefficient of a thin layer might be expressed as follows [12, 31, 42]:

$$(\alpha h\nu) = \beta(h\nu - E_g)^r \quad (6)$$

$$\& \qquad \ln(\alpha h\nu) = r \ln\left(h\nu - E_g\right) + \ln\beta \quad (7)$$

The transition exponent (r) in eqn. (6) has been determined from eqn. (7) as described elsewhere [43]. The value of (r) was found equal to ~2 for all the present compounds indicating indirect allowed transition. Using $(\alpha h\nu)^{\frac{1}{2}}$ vs $h\nu$ plots (Fig. 6), the values for the energy of the band gap (E_g) for compounds Kz1, Kz2 and Kz3 thin films were determined from extrapolations to $h\nu = 0$. The UV Vis absorption spectra of the Kz1- Kz3 thin films show absorption onsets, which are placed in the near UV range and give optical band gaps covering the 2.99 to 3.26 eV. These relatively broad band intervals are supported by the decimated π- conjugated and the non-

View Article Online
DOI: 10.1039/D6MA00174B

planar molecular structures imposed by the spiro conjunction and by the thieno[2,3- b]thiophene core.

As noted in Table 1 these values were found to be equivalent to those published for numerous conjugated organic materials.

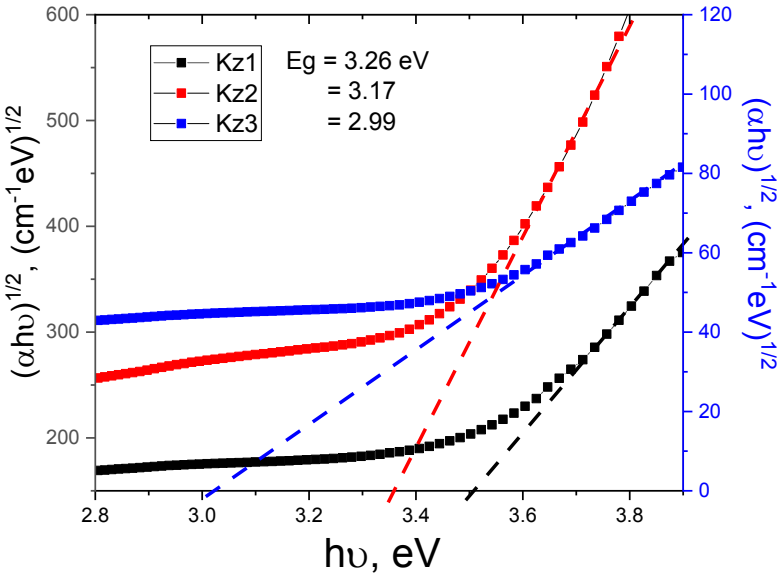

Fig. (6): $(\alpha hv)^{\frac{1}{r}} vs. hv$ plots of thin films of compounds Kz1, Kz2 and Kz3 thin films.

View Article Online
DOI: 10.1039/D6MA00174B

Table (1): The values of energy band gap E_g, Urbach energy E_u , absorption coefficient α_{500}, and refractive index n_{500} for kz1, kz2, and kz3 thin films in comparison with the corresponding reported ones.

	$\alpha_{500}(cm^{-1})$ $x10^5$	n_{500}	E_g (*ev*)	E_u *(ev)*	Reference
Compound Kz1	0.95	1.47	3.26	3.12	Present work
Compound Kz2	2.18	1.85	3.17	2.27	
Compound Kz3	2.5	1.97	2.99	0.96	
TT amino cyano + 1-naphthyl amine	3.4	1.55	2.79	1.04	[13]
3,4-diamino-N'2,N'5-bis(2-oxoindolin-3-ylidene)thieno[2,3-b]thiophene-2,5-dicarbohydrazide	5.6	1.92	2.7	1.45	[10]
3′-acetyl-5′-amino-2′-methyl-2-oxo-7'-(thiophen-2-yl) spiro[indoline-3,4′-pyrano[2,3-b]pyridine]-6′-carbonitrile	0.7	2.06	3.56	--	[12]
p-tert-Butylthiacalix[4]arene derivatives		4.2	2.9	1.23	[44]

Optical conductivity is a key measurement that tells how well a material works to carry electric charges when an electromagnetic field is moving. It gives us an improved understanding of how photons that strike the material interact with free carriers or localized states. We used the measured refractive index (n) and absorption coefficient (α) to find the optical conductivity (σ_{opt}) using the following equation [45]:

$$\frac{\alpha n c}{4\pi} = \sigma_{opt}$$

, at which c is the speed of light and λ is the wavelength.

Fig. (7) exhibits that strong interband electronic transitions close to the fundamental absorption edge cause all samples to have the highest optical conductivity in the ultraviolet wavelength range (about 400 nm). The optical conductivity gradually decreased as the wavelength increased through the visible and near-IR range, which is consistent with lower photon energy and decreasing absorption. Furthermore, compared to Kz1 and Kz3, Kz2 exhibits larger optical conductivity in the area of longer wavelength region. This suggests that there are more free carriers or defect states present, which improve sub-bandgap absorption. Kz1's lower Urbach energy and higher refractive index, on the other hand, are consistent with its comparatively lower optical conductivity at higher wavelengths, suggesting enhanced crystallinity and less structural disorder. The obtained results show that modifying the film's

View Article Online
DOI: 10.1039/D6MA00174B

composition and quality of structure may enhance its optical conductivity for optoelectronic applications, including photodetectors, and transistors, as well as absorber layers, where controlling the way light interacts with material and the way carriers move is significant for device performance.

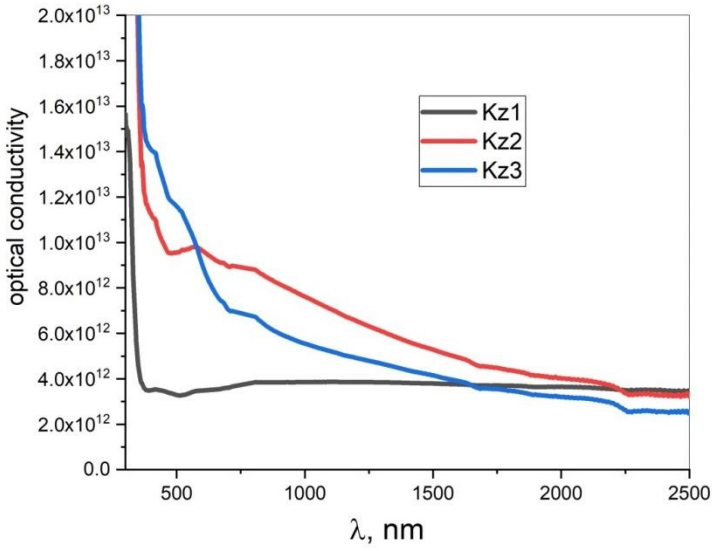

Fig. (7): Variation in optical conductivity of compounds Kz1, Kz2 and Kz3 thin films.

3.4.2. Dielectric and Dispersion characterization:

The dielectric constant (ϵ) is a crucial metric for understanding electronic transitions and excitonic properties in semiconductors [46, 47]. Materials with greater values of ϵ are endowed with inherent charge carriers [48]. In normal dispersion, ϵ' decreases with λ^2, indicating increased free carrier absorption and suggesting a gradual decline in optical absorption with increasing wavelength. The following equations can be used to calculate dielectric parameters in thin films, including the lattice dielectric constant ϵ_L, the ratio N/m of carrier concentration N to m (m is the ratio m^*/m_o of carrier effective mass to the electron rest mass), the contribution of free carriers susceptibility χ_c to the real dielectric constant, and the plasma frequency ω_p [49]:

$$\epsilon' = n^2 - k^2 = \epsilon_L - \frac{e^2}{\pi c^2 m_o} \times \left(\frac{N}{m}\right)\lambda^2$$

$$= \epsilon_L + 4\pi\chi_c \quad (8)$$

$$\omega_p = \frac{2\pi C}{\lambda_p} = \left(\frac{Ne^2}{\epsilon_o m_o}\right)^{1/2} \quad (9)$$

$$\& \quad N = \frac{\epsilon_o m_o}{e^2}{\omega_p}^2 \quad (10)$$

View Article Online
DOI: 10.1039/D6MA00174B

, where λ_p is the plasma wavelength (the λ value at $\epsilon' = 0$), e is the electronic charge, and c is the speed of light. The results showed that compound Kz2 had high dielectric characteristics, which might be attributable to its large absorption. Table 2 contains the computed dielectric parameters based on the ϵ' - λ^2 graphs in Fig. (8.a).

Di Domenico and Wemple [50] proposed a single oscillator model to explain the relationship between refractive index and photon energy in the normal dispersion region. The equation is as follows:

$$(n^2 - 1)^{-1} = \frac{E_o}{E_d} - \frac{1}{E_o E_d}(h\nu)^2 \qquad (11)$$

, E_o and E_d are the oscillator and dispersion energies, respectively.

Figure (8.b) depicts the $(n^2 - 1)^{-1}$ vs. $(h\nu)^2$ plots for compound kz1, kz2 and kz3 thin films. The oscillator energy E_o and dispersion energy E_d can be derived from the slope $(E_o E_d)^{-1}$ of the linear component of the plot and the intercept (E_o/E_d) with the ordinate axis, where $E_o = \left(\frac{intercept}{slope}\right)^{1/2}$ & $E_d = (\text{slope} \times \text{intercept})^{-1/2}$

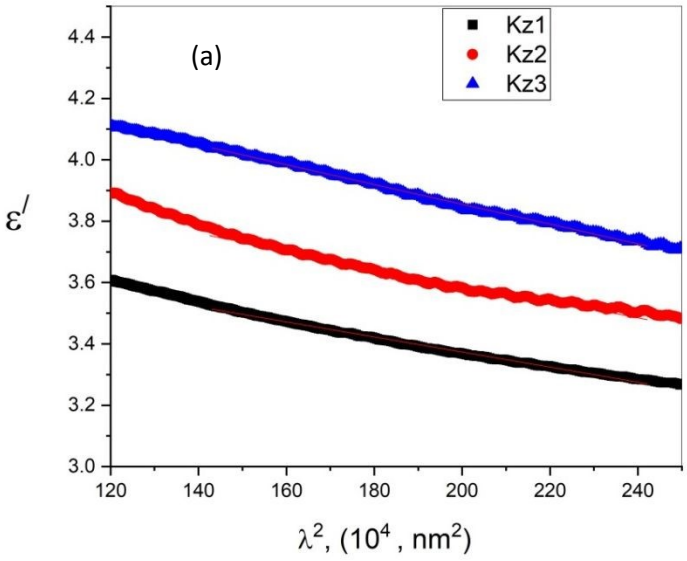

View Article Online
DOI: 10.1039/D6MA00174B

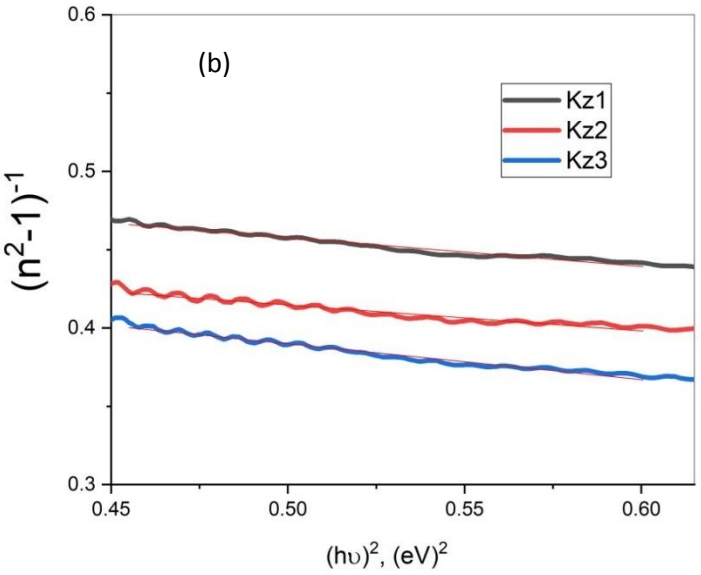

Fig. (8): ϵ' - λ^2(a) and ϵ'' - λ^2 (b) plots for thin films of compounds Kz1, Kz2 and Kz3 thin films..

The dielectric and dispersion properties have been documented and compared with those of several conjugated organic compounds, as presented in Table 2.

Table 2: Comparing of the dielectric and dispersion properties of the current samples against the ones reported before.

	E_o (eV)	E_d (eV)	ϵ_L	N/m* (10^{17} cm^{-3} g^{-1})	|χc|	ω_p, s^{-1} × 10^{14}	References
Compound Kz1	1.74	3.17	3.86	2.74	0.74	12.0	Present Work
Compound Kz2	1.75	3.57	4.14	3.06	0.75	12.5	
Compound Kz3	1.77	3.94	4.49	3.47	0.77	12.8	
PPY film	2.37	--	2.94	0.95	0.32	5.52	[38]
TT amino ester	2.15	2.95	3.29	0.034	0.16	3.31	[51]
Diethyl3,4-bis(((E)-2- xoindolin-3-ylidene)amino)thieno[2,3-b]thiophene	2.16	3.86	4.47	0.057	0.27	1.35	[5]
3,4-diamino-N'2,N'5-bis(2-oxoindolin-3-ylidene)thieno[2,3-b]thiophene-2,5-dicarbohydrazide	4.5	2.7	4.51	0.86	0.034	5.25	[10]
TT amino cyano + 1-naphthyl amine	2.29	5.45	5.61	-	0.44	--	[13]

View Article Online
DOI: 10.1039/D6MA00174B

3.4.3. Thermoelectric characterization and performance:

The typical interrelation of the Seebeck coefficient and electrical conductivity, which are functions of charge carrier concentration and mobility, makes it is essential to identify the electrical transport mechanism in the present organic compounds. Figure 9a depicts the DC-electrical resistance (R) for compounds Kz1, Kz2, and Kz3 thin films at temperatures ranging from 437 to 553 K. The original Kz1, Kz2, and Kz3 thin films have a comparatively high overloaded resistance at RT due to their gluttonous tendency to oxygen absorption. Furthermore, the adsorbed atmospheric oxygen molecules can grab n-type conduction electrons, reducing electron concentration and resulting in an overloaded amount of film resistance. The measurable R-values of 21 x 10^7 Ω were achieved at ~ 437 K, and decreased to 11 x 10^6, 10.3 x 10^6, and 10 x 10^6 Ω for Kz1, Kz2, and Kz3 compound thin films, respectively, at ~ 553 K, indicating semiconducting behavior.

This may demonstrate that the adsorbed oxygen can be thermally liberated over the film surface, leading to an increase in sample conductivity.

The following Arrhenius relationship [52-54] may calculate the conduction activation energy in the visible resistance ranges, where;

$$\sigma_{DC} = \sigma_1 \exp\left(\frac{-\Delta E_{\sigma_1}}{K_B T}\right) + \sigma_2 \exp\left(\frac{-\Delta E_{\sigma_2}}{K_B T}\right) \quad (12)$$

ΔE_{σ_1} & ΔE_{σ_2} and σ_1 & σ_2 represent the thermal activation energies associated with the conduction and the pre-exponential factors corresponding to lower and higher temperature ranges, respectively. While K_B is the Boltzmann's constant. Figure 9b reveals that the graphs of lnσ vs.1000/T have been straight. The activation energy for electrical conduction represents the energy barriers which charge carriers must overcome in order to flow. Compound Kz1, Kz2, and Kz3 thin films have ΔE_{σ_1}, ΔE_{σ_2} values of (0.76, 0.40), (0.72, 0.36) and (0.57, 0.16), in the lower and higher temperature ranges, respectively. Compound Kz1 has the highest activation energy value, suggesting that charge carriers need higher amounts of energy to become mobile. On the other hand, the compound Kz3 thin film has the lowest activation energy, which could be ascribed to the continuous conjugation effect, which increases hopping conduction. The values of ΔE_σ are similar to computed values for various organic semiconductor materials [55, 56].

View Article Online
DOI: 10.1039/D6MA00174B

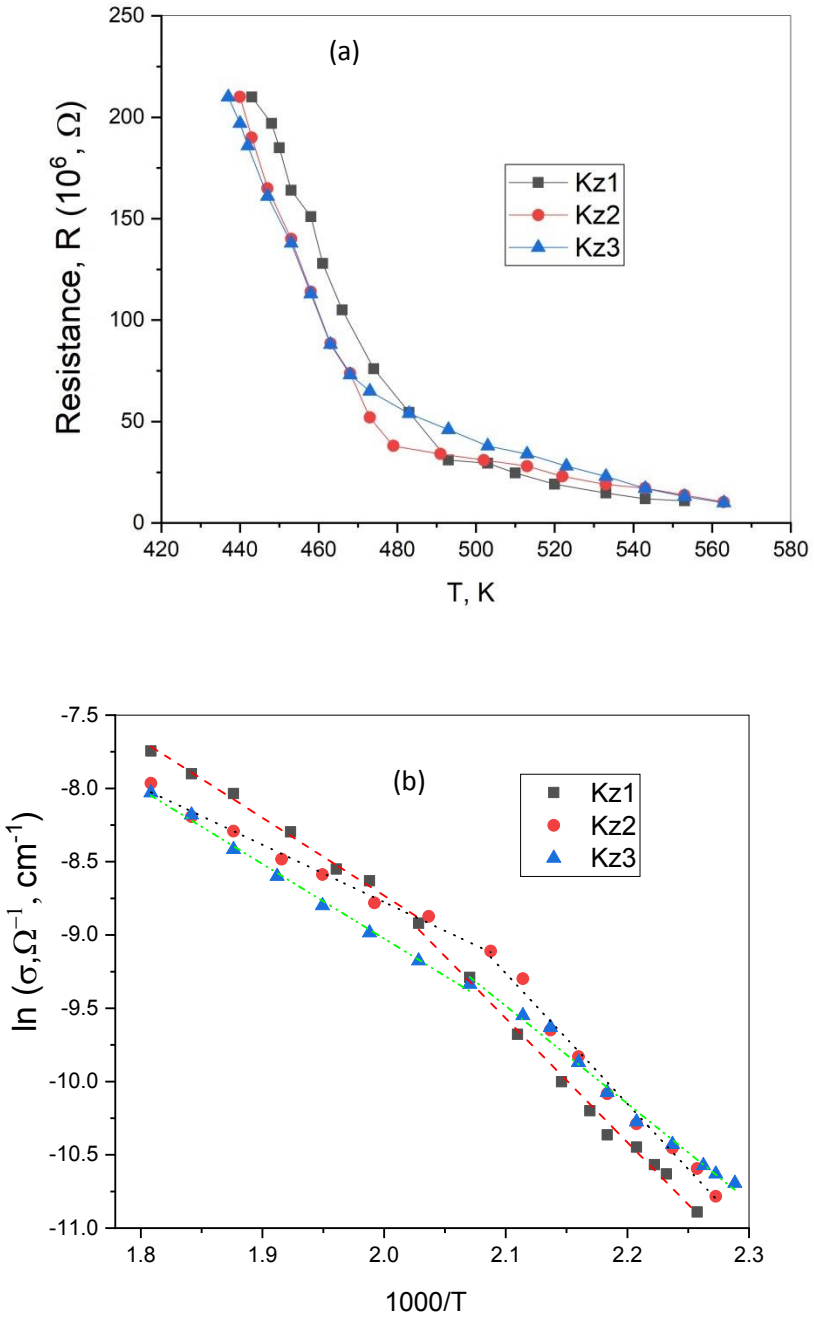

Fig. (9): Plots of DC-electrical resistance R vs. T (a) and ln (σ_{DC}) vs. (1000/T) (b) for compound Kz1, Kz2, and Kz3 thin films.

The Seebeck coefficient is an extremely important thermoelectric material property. It is the voltage generated by a material when a temperature differential exists. The Seebeck coefficient, (μV/K - mV/K), indicates the charge carriers (either holes or electrons) flow from the hot side to the cold side of the sample that causes the potential (voltage) decrease. The Seebeck

View Article Online
DOI: 10.1039/D6MA00174B

coefficient also dictates the charge carrier type (positive charge carriers - holes, negative charge carriers - electrons) as well as if the material is having degenerate or non-degenerate transport properties.

3.4.4. Structure–property analysis

The distinctions of the thermoelectric behaviors in Kz1, Kz2 and Kz3 can be explained by the molecular structures and conformations of the synthesized compounds. Kz2 takes a linearly expanded coil geometry, as shown in Scheme 1, whilst Kz1 and Kz3 have smaller geometries. This extended structure in Kz2 allows interchain $\pi - \pi^*$ stacking and is good at charge carrier mobility as indicated by the higher electrical conductivity and the power factor of Kz2 relative to the other two substances. This stiffness of the spirothiadiazole-thieno[2,3-b]thiophene unit of Kz1 contributes to a higher threshold to electrical conduction (ΔE_{σ_1} = 0.76 e V) and therefore the conductivity is lower. Conversely, Kz3, even with a benzimidazole group atom, has seen an intermediate performance because of the presentation of a disulfide bond that partially breaks the conjugated performance. Such observations put a stress on the concept that thermoelectric performance cannot just be determined by the total length of the π -conjugation, but is instead largely determined by the molecular structure, and the level of order within the thin film.

The electrical and thermal properties of a thermoelectric material can be correlated through the figure of merit z, K^{-1} or the dimensionless zT, where:

$$\frac{s^2}{\rho k} z = \quad (13)$$

$$\& \qquad zT = \frac{s^2 T}{\rho k} = \frac{(S_n - S_p)^2 T}{\left[(\rho_n k_n)^{\frac{1}{2}} + (\rho_p k_p)^{\frac{1}{2}}\right]^2} \quad (14)$$

, where $S, \rho \& k$ are Seebeck coefficient, electrical resistivity and thermal conductivity, respectively, and $T = [T_h + T_c]/2$ is the average temperature between the temperature T_h and T_c of the hot and cold sides, respectively, n& p refers to n – and p - semiconductors. zT typically indicates the thermoelectric performance.

The ideal thermoelectric materials are characterized by low values of both k and ρ to increase the temperature gradient and decrease Joule heat, respectively. This leads to maximizing the participation of the obtainable charge carriers in the thermoelectric effect. Besides, the

View Article Online
DOI: 10.1039/D6MA00174B

Seebeck coefficient S depends on the Fermi – level energy position and material structure that is affected mainly by the charge carrier density and temperature. Moreover, the thermal conductivity $\hbar$ of a material results from lattice vibrations (phonons) $\hbar_l$ and charge carrier (electron) $\hbar_e$ components.

$$\hbar_e + \hbar_l \hbar = i.e \quad (15)$$

Thermal Conductivity Estimation Method

According to Wiedemann – Franz law [57, 58] was used to estimate the total thermal conductivity $\hbar_e$ in this research, the electronic thermal conductivity $\hbar_e$ is generally proportional to the electrical conductivity σ. For organic materials, this law is often represented by:

$$\hbar_e = LT\sigma \quad (16)$$

, where $L = 2.44 \times 10^{-8} W\Omega/K^2$ is the Lorenz number.

In accordance with the decrease of both S and ρ while $\hbar_l$ increases with increasing the charge carrier's concentration, the metals reveal small values of zT unlike insulators that possess relatively high values of zT due to their small $\hbar$ and high ρ & S values. This encourages us to expect that the optimal carrier concentration values could be almost close to $10^{17} - 10^{19}\ cm^{-3}$ characterizing the range of the critical case between the degenerate and non – degenerate semiconductors. Due to the fact that $\hbar_e$ was not determined experimentally, the values of zT are not the real values but the approximated upper limits. However, since the similar estimation technique was implemented across all the samples, the comparative trends among Kz1–Kz3 and under different treatment conditions remain valid. The heat conductivity of organic semiconductors is normally dominated by the lattice thermal conductivity; thus, the values of the zT are reported as upper-bound values but not as absolute values.

3.4.5. Optimization of thermoelectric performance:

In order to maximize the TE – performance, different ways such as optimizing concentration, enhancing carrier mobility and / or electrical and thermal conductivities comprising can be employed. Herein, the present organic compounds with different conformations and conjugation numbers and consequently different carrier concentrations had been examined at different temperatures.

As shown in Fig. (9& 10) the simultaneous increase and decrease of σ and S, respectively, with elevating temperature could be attributed to the mixed conduction (by both

View Article Online
DOI: 10.1039/D6MA00174B

electrons and holes) and give an impression that their behaviors are assigned to the same factors. These results can be described by the following two unlike carrier's mechanisms [40], where;

$$\sigma = en\mu_n + ep\mu_p = en\mu_n\left[1 + \left(\frac{p}{n}\right)\left(\mu_p/\mu_n\right)\right] \quad (17)$$

$$\& \quad (-S) = \frac{|S_n|\mu_n n - |S_p|\mu_p p}{\mu_n n + \mu_p p} = \frac{|S_n| - |S_p|\left(\mu_p/\mu_n\right)\left(\frac{p}{n}\right)}{1 + \left(\mu_p/\mu_n\right)\left(\frac{p}{n}\right)} \quad (18)$$

, where S_n, μ_n & n and S_p , μ_p & p are the Seebeck coefficient, mobility and density of electrons and holes, respectively. Thus, the changes in σ and S with elevating temperature are associated with the changes in p/n and/or μ_p/μ_n ratios caused by temperature.

The S – T plots given in Fig. (10a) show that the Seebeck coefficient values of Kz1, Kz2 and Kz3 thin films are relatively high (mV/K units), which are comparable to S – values for some inorganic materials [59-61]. Besides, the negative sign of S is indicative to n-type thermoelectric materials. If large, the Seebeck coefficient also indicates the Fermi level is very low below the conduction band edge, generally relating to lower carrier densities or more energy-dependent scattering. The different values obtained for the Seebeck coefficient by the present compounds may mainly depend on the different conjugation numbers in the compounds' structures. As shown in Table 3, the Kz2 compound thin film has the largest negative Seebeck coefficient values of - 0.71 mV/K and - 0.85 mV/K indicating extensive thermoelectric voltage generation. These good thermoelectric results attained by compound Kz2 among others, are expected. That is because compound Kz2, unlike the others, contains a larger conjugation number with a linearly expanded coil conformation (scheme1). Such stretch conformation is considered an effective method for improving the TE – performance of organic materials by enhancing their carrier mobility [62-65].

Besides, the temperature dependence shows that there is a moderate to very large increase of the Seebeck coefficient size during temperature increase, specifically for Kz1, Kz2, and Kz3, and which is indicative of a non-degenerate semiconductor's behavior [66]. This illustrates that the heating of the carriers is a significant factor in the transport process.

To confirm whether the charge carrier system in the organic compounds, which are physically regarded as often amorphous semiconductors, is degenerate or non-degenerate, the concept of the Fermi level could be utilized. It is represented by the chemical potential of

View Article Online
DOI: 10.1039/D6MA00174B

electrons in the system at 0 K, and separated from the conduction band minimum value E_c (LUMO) by the energy value E_f that can be termed the carrier activation energy [67, 68] .

The degeneracy of the electron gas is the case in which the number of carrier particles is comparable to the number of allowed states, i.e., when the probability Fermi function $f(E)$ approaches unity;

$$f(E) = \frac{1}{e^{(E-E_f)/kT}+1} \cong 1 \quad (19)$$

, where $E = E_c = 0$ for n – type semiconductor.

This means that $e^{E_f/kT} \gg 1$ and E_f has a positive value. While the electron gas is non – degenerate when $f(E) \ll 1$ and $e^{E_f/kT} \ll 1$ or E_f has a negative value.

Besides, Fermi – level energy E_f can be correlated to Seebeck coefficient through the following Benco and Koffyberg [69];

$$S = \frac{k_B}{e}\left(\frac{E_f}{kT} + A\right) \quad (20)$$

Or

$$\frac{E_f}{kT} = \frac{|S|e}{k_B} - A \quad (21)$$

, where e is the electronic charge, k_B is the Boltzmann's constant and A is a dimensionless constant that depends on the scattering mechanism. A = 1 for amorphous materials [18, 19 same].

Fig. (10b) gives the $|S|$ versus 1000/T (K^{-1}) plots. As shown, the slope $\frac{k_B}{e}\left(\frac{E_f}{kT}\right)$ is negative characterizing the non - degenerate n – type semiconductor [59]. The calculated values of $e^{E_f/kT}$ using eq. (21) are given in Table 3 for compounds Kz1, Kz2, and Kz3 at different temperatures corresponding to the lower and higher temperature ranges, respectively.

The majority carrier (electrons) concentration *N* for each compound was determined using the following relation [70];

$$N = \frac{2(2\pi m k_B T)^{3/2}}{h^3} e^{E_f/kT} \quad (22)$$

The calculated values of *N* at different temperatures in the relatively lower and higher temperature ranges for Kz1, Kz2, and Kz3 are given in Table (3). As shown, the results of S and $e^{E_f/kT}$ for the present compounds are characteristics of non – degenerate n – type semiconductors. Table (3) and Fig. (11) summarize and compare the TE – results of the present three compounds. As shown, the TE – figure of merit zT attained by Kz2 compound is the best among the other of the present compounds. That is due to an optimum interaction of carrier

View Article Online
DOI: 10.1039/D6MA00174B

concentration, carrier mobility as well as molecular conformation and not only to a long π-conjugation length.

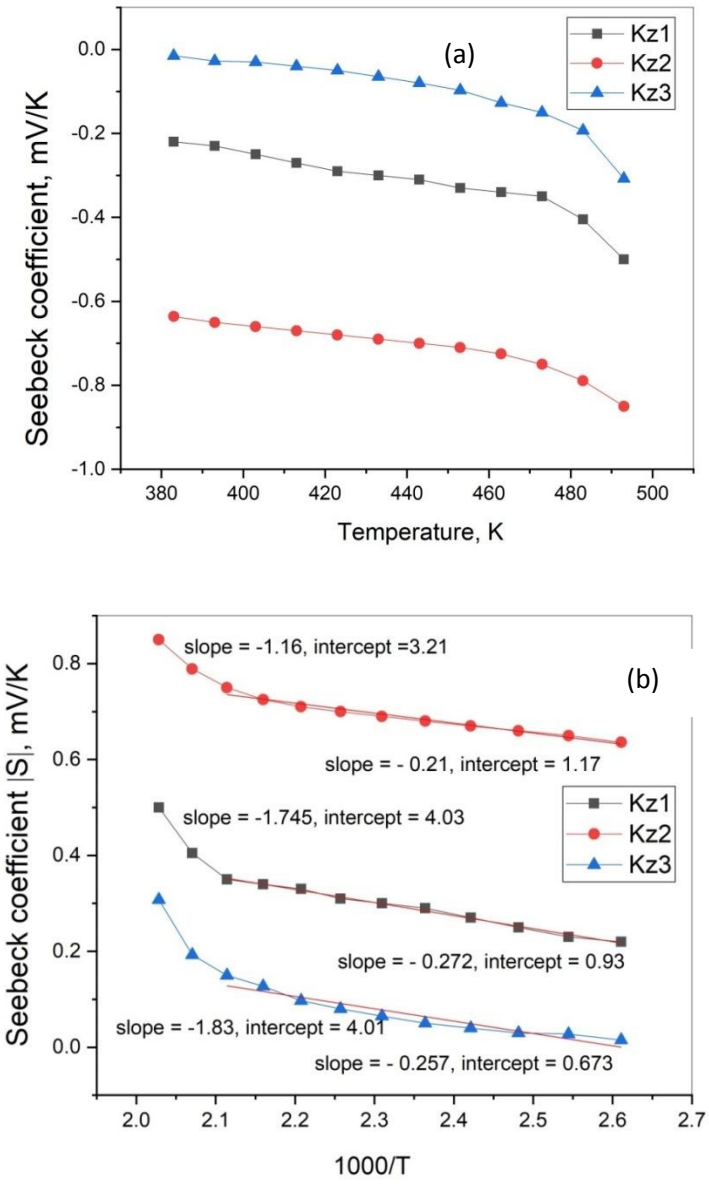

Fig. (10): Seebeck coefficient *vs* temperature plots for compound Kz1, Kz2, and Kz3 thin films.

Table 3: the average values of Seebeck coefficient of the present compounds over the considered temperature ranges

Sample	T (K)	$\sigma(\Omega cm)^{-1}$	-S (mV/K)	$e^{E_f/kT}$	N, cm^{-3}	zT
Kz1	453	2.90	0.097	0.01	5.34×10^{17}	0.18

View Article Online
DOI: 10.1039/D6MA00174B

	463	3.70	0.127	0.04	2.11×10^{18}	0.19
	473	6.30	0.15	0.06	3.60×10^{18}	0.19
	483	9.20	0.193	0.08	4.84×10^{18}	0.21
	493	15.1	0.31	0.12	7.09×10^{18}	0.24
Kz2	453	3.40	0.71	1.92×10^{-5}	1.00×10^{17}	0.57
	463	5.38	0.72	2.56×10^{-5}	1.38×10^{17}	0.59
	473	9.15	0.75	6.11×10^{-5}	3.41×10^{17}	0.59
	483	12.1	0.83	8.66×10^{-5}	4.99×10^{17}	0.62
	493	17.2	0.85	9.73×10^{-5}	5.78×10^{17}	0.67
Kz3	453	3.45	0.31	0.001	5.82×10^{16}	0.10
	463	4.21	0.33	0.002	1.20×10^{17}	0.12
	473	6.52	0.35	0.006	3.35×10^{17}	0.14
	483	8.81	0.44	0.007	4.60×10^{17}	0.18
	493	10.3	0.50	0.008	5.99×10^{17}	0.20

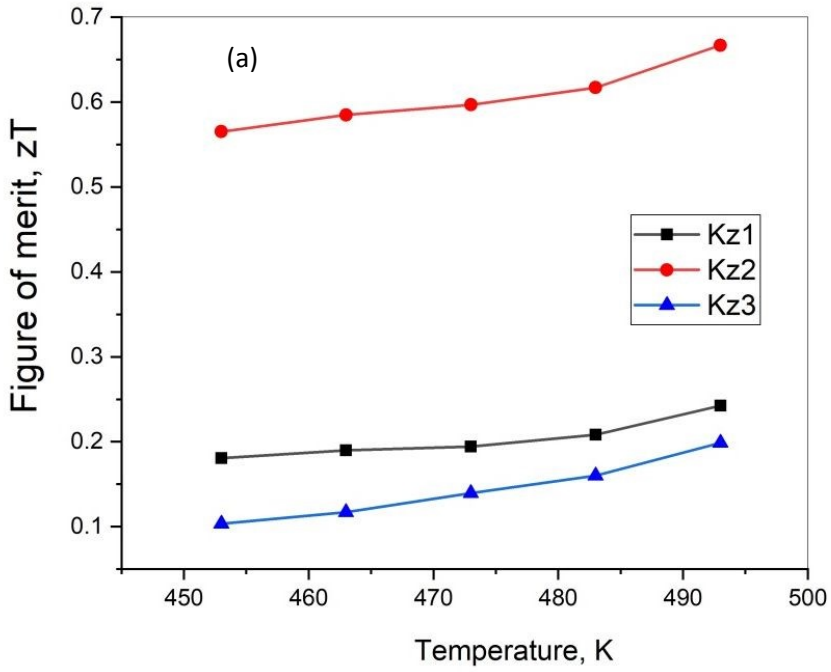

View Article Online
DOI: 10.1039/D6MA00174B

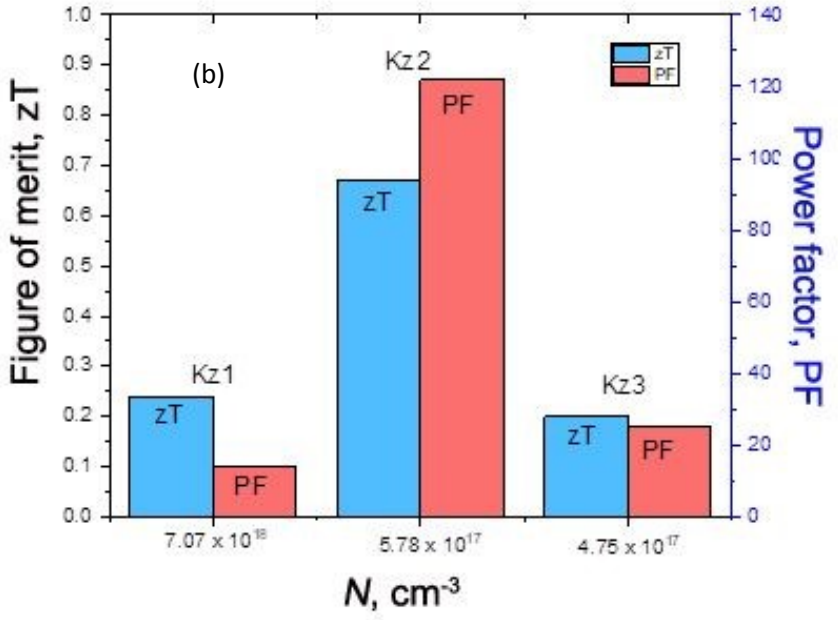

Fig. (11): zT vs. T plots (a), and zT & PF at optimal carrier concentrations values (at T = 493 K, $\Delta T \sim 4$℃) (b) for Kz1, Kz2, and Kz3 compound thin films

More TE – performance improvement of Kz2 compound thin film has been tried through carrier concentration optimization. The increase or decrease of charge carriers (electrons) could be achieved by annealing or oxidizing gas (Iodine) doping, which causes excitation or trapping of electrons, respectively.

Fig. (12a) shows that the carrier density, in general, increases with elevating temperature. However, the film treatments by iodine exposure and annealing at 150 °C for 5 min have led to strong and slight declines in *N* values compared to its values for the pristine film, which could be mainly attributed to the trapping of electrons by iodine and the scattering increase with temperature, respectively. This change in *N* has similarly impacted on the values of all TE – parameters as seen in Fig. 12 (b, c, d& e). Besides, elevating the annealing temperature to 200 ℃ has resulted in evident improvements in all TE – parameters. This enhancement in PF and zT values can be attributed to the Kz2 compound crystallinity improvement by annealing. X- Ray diffractograms given in Fig. (13) for as - deposited and annealed (200℃ , 10 min) reveal the appearance multiple sharp peaks after annealing, which represent the compound structural fingerprint. This may indicate that the thienothiophenes-based compound becomes crystalline

View Article Online
DOI: 10.1039/D6MA00174B

after annealing, where the C, H, and O atoms contained in the compound can be arranged together in the crystal lattice.

Besides, the relatively smaller value of zT of the film annealed at 200℃ for 10 min compared with its value after annealing for the shorter time of 5 min is due to the higher value of thermal conductivity caused by the longer time of annealing (Fig 11e). Such an annealing effect may indicate that the annealing is an essential impacting factor in TE – parameter compromise. This conclusion can be emphasized by the summarized TE – results given at different conditions in Table (4) and Fig. (14).

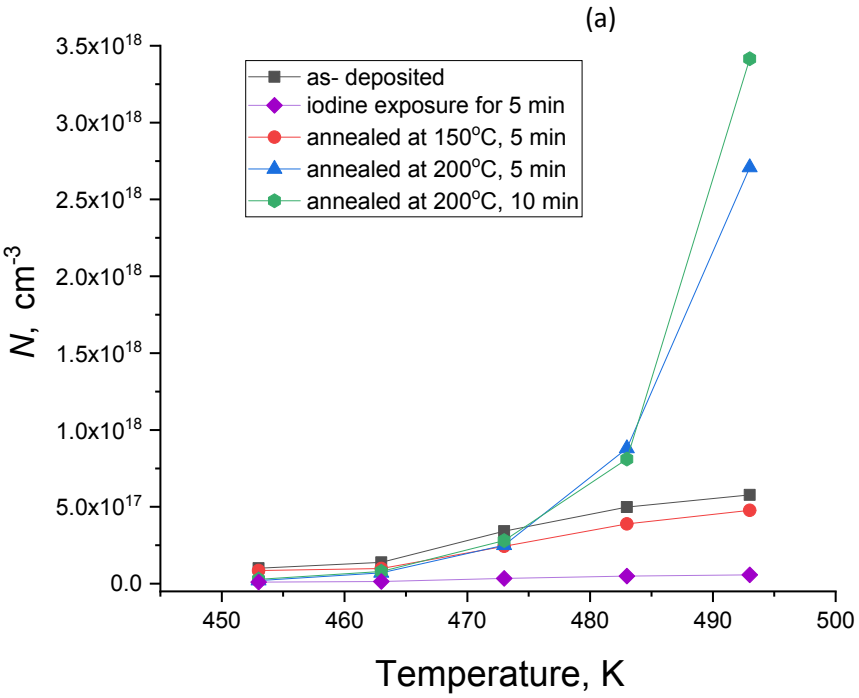

View Article Online
DOI: 10.1039/D6MA00174B

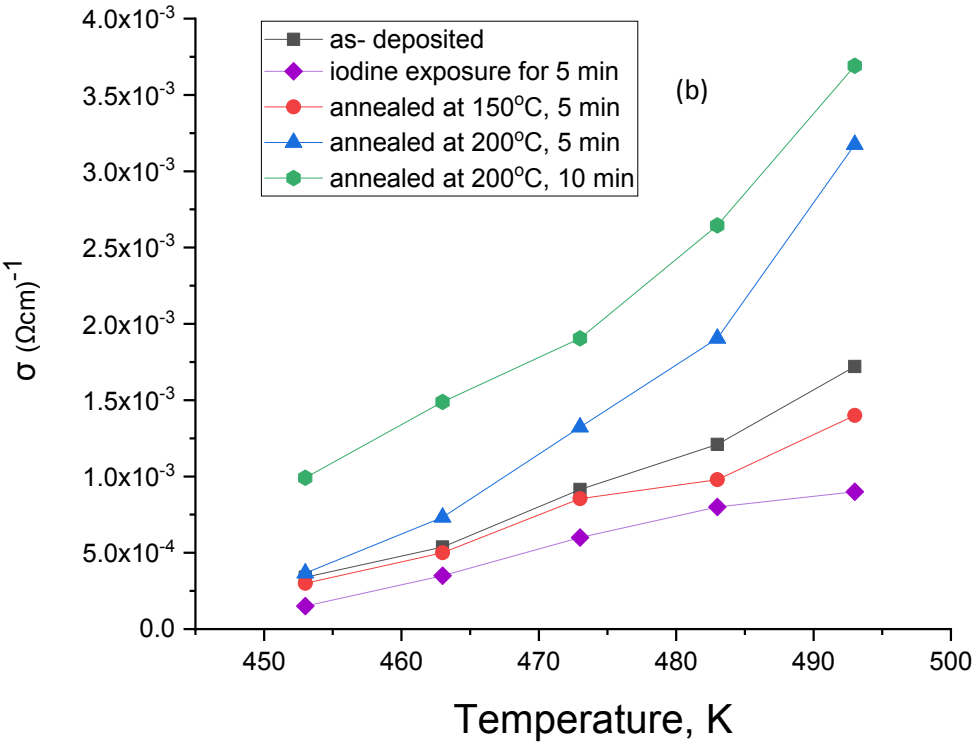

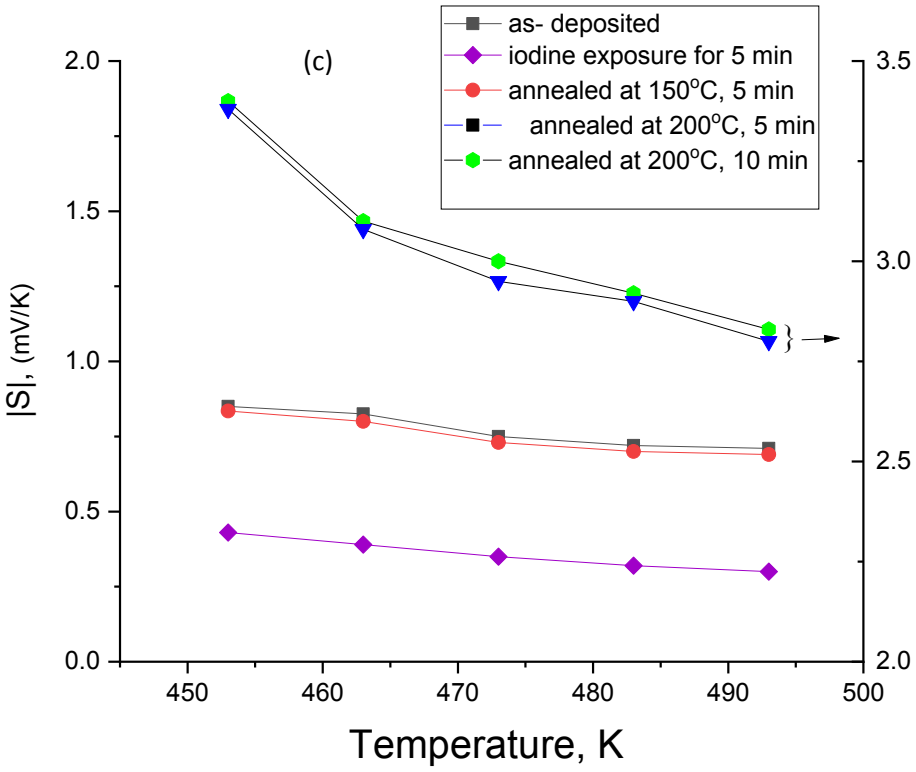

View Article Online
DOI: 10.1039/D6MA00174B

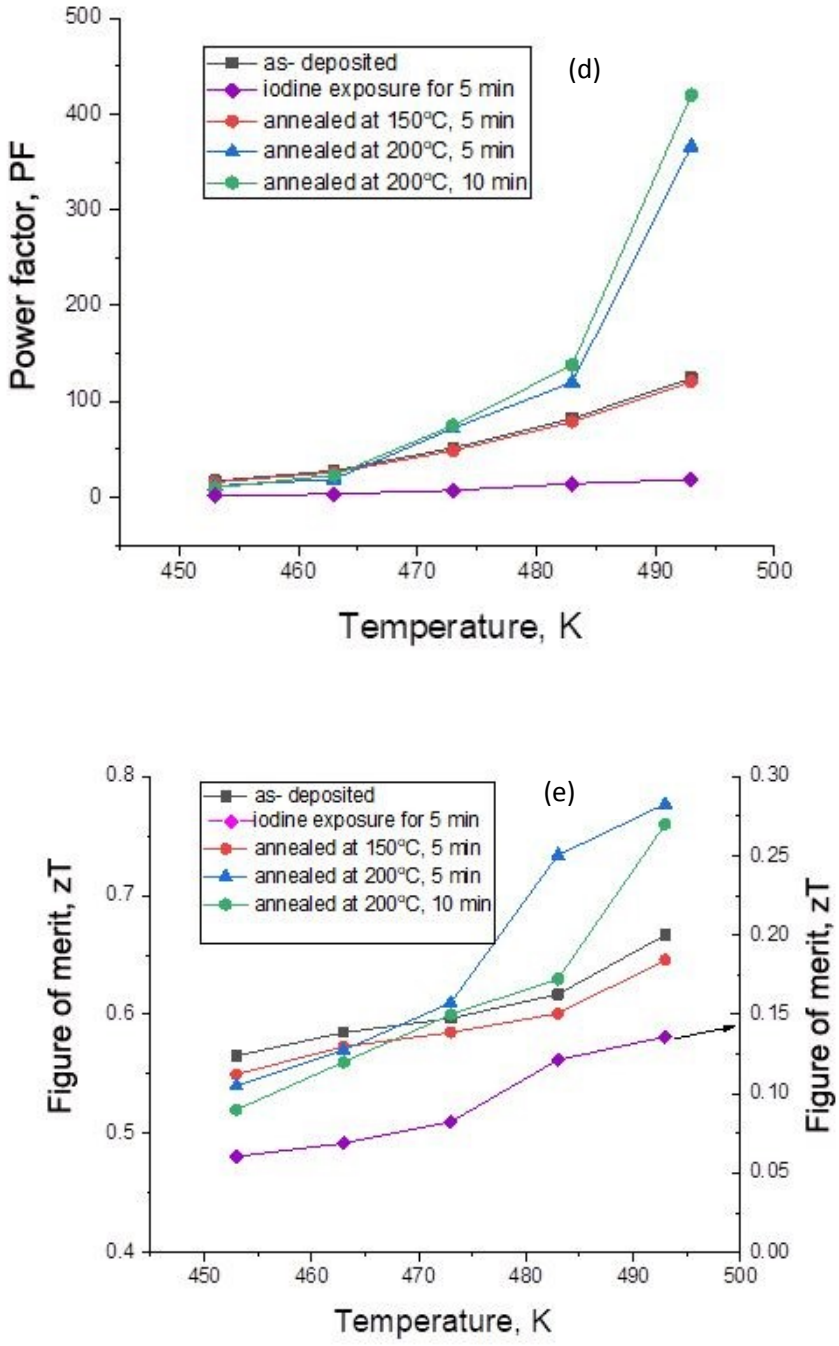

Fig. (12): variations of N, cm^{-3} (a), σ, $(\Omega.cm)^{-1}$ (b), S, mV/K (c), PF $(\mu W/m{-}K^2)$ (d) and zT (e) for Kz2 compound thin film at different conditions.

View Article Online
DOI: 10.1039/D6MA00174B

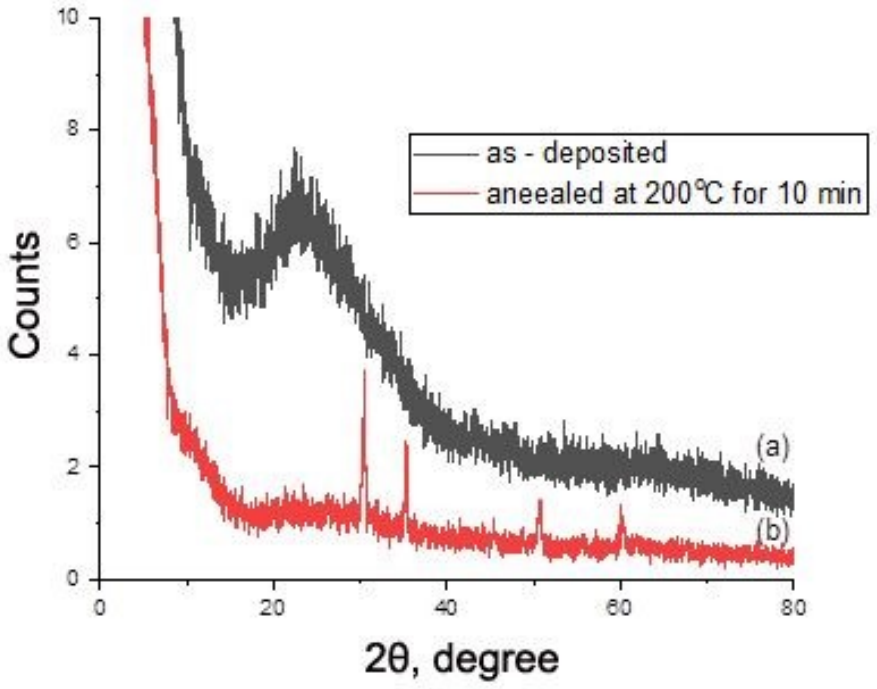

Fig. (13): X – ray diffractogarms of as – deposited (a) and annealed at 200℃ for 10 min (b) for Kz2 compound thin films.

Table (4): TE – parameters of Kz2 at different conditions θ

Sample	T (K)	$\sigma(\Omega cm)^{-1} \times 10^{-4}$	-S (mV/K)	$e^{E_f/kT}$	N, cm^{-3}	zT	PF
Kz2 (as- deposited)	493	17.2	0.85	9.73×10^{-5}	5.78×10^{17}	0.67	124
Kz2 (exposure to I_2 gas, for 5 min)	493	0.92	0.43	2.56×10^{-5}	1.38×10^{15}	0.14	18
Kz2 (annealing at 150℃ for 5 min)	493	14.4	0.835	8.66×10^{-5}	4.63×10^{17}	0.65	100
Kz2 (annealing at 200 ℃, for 5 min)	493	31.7	3.4	0.11	3.41×10^{18}	0.78	366
Kz2 (annealing at 200 ℃, for 10 min)	493	36.9	3.38	0.087	2.70×10^{18}	0.77	421

View Article Online
DOI: 10.1039/D6MA00174B

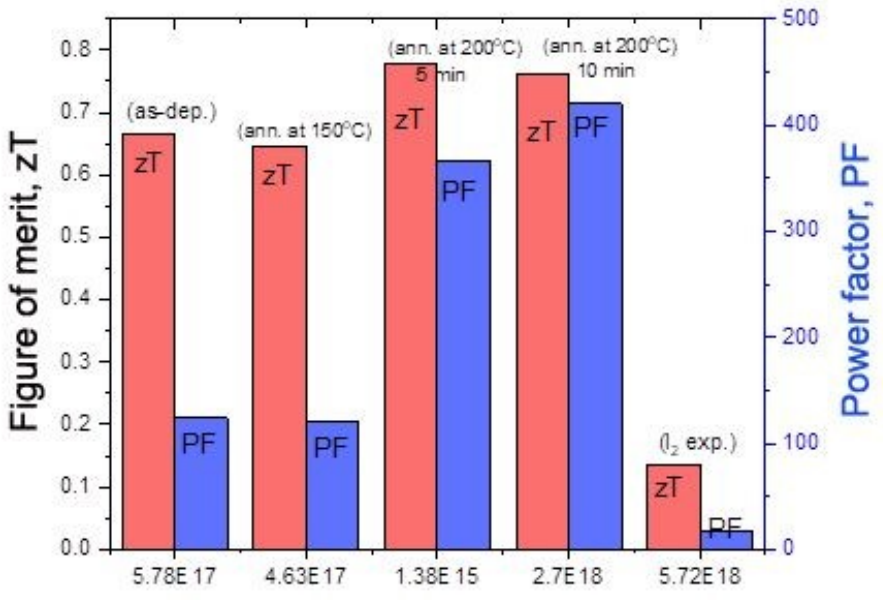

Fig. (14): Comparison of the optimal values of thermoelectric zT and PF parameters at different conditions for Kz2 compound thin film

Thermoelectric figure of merit (zT) was determined by using the experimentally determined electrical conductivity and Seebeck coefficient, and the thermal conductivity was determined by the Wiedemann Franz relation. It should be mentioned that in organic semiconductors, lattice vibrations are the main heat carriers, and the overall thermal conductivity is usually between 0.1 and 0.5$Wm^{-1}K^{-1}$. In the current research, the lattice thermal conductivity was not measured experimentally because of the limitations of the experiment, and thus, the reported zT numbers should be treated as estimated upper limits but not exact ones. However, as the same assumptions and calculating process had been used in all samples, the comparative tendencies of thermoelectricity are still viable. The improved value of zT in Kz2 following thermal annealing in this case is an indication of its desirable balance between electrical conductivity and Seebeck coefficient and not an exaggeration due to thermal conductivity approximation. Moreover, it is notable that the environmental stability of the synthesized compounds during the ambient conditions in the long run was not investigated in the current study. That is why, they are not device ready thermoelectric materials and these materials are proof-of-concept systems that are intended to shed light on the structure-property relations that conform thermoelectric performance. Lattice thermal conductivity would be directly determined

View Article Online
DOI: 10.1039/D6MA00174B

by systematic evaluation of shelf-life, humidity tolerance, and thermal cycling stability, rational evaluation of lattice thermal conductivity would be systematically assessed.

A comparison of the optimized TE – PF and zT parameters of Kz2 compound with others reported for some materials is given in Table (5). It is pronounced that either PF and/or zT values of the present kz2 compound are better than the corresponding ones of most of the tabulated materials. However, more or less, the values of zT of the present Kz2 organic compound can be competitive in thermoelectric applications due to its cost and scalability advantages over inorganic ones.

Table (5): comparison of the values of thermoelectric PF and zT parameters of Kz2 compound with the reported ones of some other materials

	T(K)	zT	P.F. = $S^2\sigma$ ($\mu W/m-K^2$)	Ref.
Kz2 (as- deposited)	493	0.67	124	Present work
Kz2 (annealed - 200 ℃, for 5 min)	493	0.78	366	
Kz2 (annealed - 200 ℃, for 10 min)	493	0.77	421	
Type (I)-p (Bi0.5Sb1.5Te3)	373	1.3	34	[70]
Type (II)-p (Bi0.4Sb1.6Te3)	373	1.25	47	[70]
p-PbTe(Mg, Na)	800	1.67	24.1	[71]
Tetrakis(dimethylamino)ethylene	400	0.5	1040	[72]
Ethylene glycol-mixed PEDOT:PSS	300	0.28	350	[73]
Poly[Na_x(Ni-1,1,2,2-ethenetetrathiolate)s]	440	0.1	27.62	[74]
PEDOT:PSS/SWCNT TE thin films	350	0.43	501.31 ± 19.23	[75]
PEDOT:PSS TE fibers	300	0.27	147.8	[76]
Mixing of RN120-SWCNTs with P1. RN120-SWCNT (G2)	300	--	96.8	[77]
polymer poly(benzodifurandione) benzodipyrandione (BPDO) (PBFDO)	400	0.25	142	[78]

Summary and conclusions:

Three spirothiadiazole–thienothiophene-based macroheterocyclic compounds (Kz1–Kz3) have been synthesized under eco-friendly conditions, optically and electrically characterized and structurally confirmed. The thin films prepared by spin coating prove their quality. The as-deposited films exhibit amorphous structure and transform to semi-crystalline ones after annealing. This structural transition from amorphous to crystalline, which is beneficial for the film's electrical and thermoelectric property improvements, is emphasized by the presence of

View Article Online
DOI: 10.1039/D6MA00174B

sharp X – ray diffraction peaks for annealed film. The films exhibit relatively high transparency in the visible and NIR regions and substantial absorption in the UV. The optical band gaps range from 2.99 to 3.26 eV with indirect allowed transitions which are dependent on π-conjugation. The refractive index and extinction coefficient have typical behavior. A high dielectric constant and polarizability refer to strong electronic transitions and good light–matter interaction. Overall, results indicate promise for the synthesized materials to be a material option in optoelectronic and photonic devices. Seebeck coefficients with negative values verify electrons as the major charge carriers. The electrical conductivity steadily increased with temperature, reflecting the typical thermally activated transport characteristic of organic semiconductors. Among evaluated materials, the Kz2 compound exhibited the most promising thermoelectric performance with a power factor of 366 μW m^{-1} K^{-2} and a zT of 0.78 at 493 K after a 5-minute anneal treatment of 200 °C. This improved performance can be attributed to the fact that the coil shape of Kz2 is expanded linearly resulting in a coil shape that is easier to transport charge carriers, and that the concentration and crystallinity of the carrier improves through the annealing of the material. Although the values of the zT in this case are estimated upper limits based on using the Wiedemann Franz law of finding the thermal conductivity, this methodology is consistent, and the availability to compare samples in a meaningful way. On the whole, the findings have defined a direct relation between the molecular structure, conjugation, conformation, and thermoelectric performance that spirothiadiazole–thienothiophene macroheterocycles are potential candidates of multifunctional organic materials in flexible energy harvesting and optoelectronic technology.

Declaration of Competing Interest

The authors declare that they have no known competing financial interests or personal relationships that could have appeared to influence the work reported in this paper.

Data Availability Statement

The authors declare that the data supporting the findings of this study are available within the paper.

View Article Online
DOI: 10.1039/D6MA00174B

References:

1. A. Facchetti, π-Conjugated polymers for organic electronics and photovoltaic cell applications. *Chem. Mater.* **2011,** *23* (3), 733-758.
2. C. Liu, L. Shao, S. Chen, Z. Hu, H. Cai and F. Huang, Recent progress in π-conjugated polymers for organic photovoltaics: solar cells and photodetectors. *Prog. Polym. Sci.* **2023,** *143*, 101711.
3. S. R. Forrest, The path to ubiquitous and low-cost organic electronic appliances on plastic. *nature* **2004,** *428* (6986), 911-918.
4. H. M. Abd El-Lateef, M. S. Kamel, M. M. Khalaf and M. A. E. A. A. Ali, Studying the effect of annealing temperature on the optical characteristics of conjugated pyrrolo [2, 3-b] pyrrole azo dye thin films for optoelectronic devices. *Opt. Mater.* **2024,** *157*, 116343.
5. H. M. Abd El-Lateef, M. S. Kamel, A. Y. A. Alzahrani, M. M. Khalaf, M. Gouda and M. A. E. A. A. Ali, Synthesis, characterization, and study of linear and non-linear optical properties of some newly thieno [2, 3-b] thiophene analogs. *Semicond. Sci. Technol.* **2024,** *39* (12), 125014.
6. C. Bizzarri, E. Spuling, D. M. Knoll, D. Volz and S. Bräse, Sustainable metal complexes for organic light-emitting diodes (OLEDs). *Coord Chem Rev* **2018,** *373*, 49-82.
7. P. G. V. Sampaio and M. O. A. González, A review on organic photovoltaic cell. *Int. J. Energy Res.* **2022,** *46* (13), 17813-17828.
8. H. Sirringhaus, Device physics of solution-processed organic field-effect transistors. *Adv. Mater.* **2005,** *17* (20), 2411-2425.
9. Y. Liu; J. Zhao; Z. Li; C. Mu; W. Ma; H. Hu; K. Jiang; H. Lin; H. Ade; H.Yan, Aggregation and morphology control enables multiple cases of high-efficiency polymer solar cells. *Nat.Commun.* **2014,** *5* (1), 5293.
10. A.M. Soliman; M. Abd El Aleem Ali Ali El-Remail; M. S. Kamel; A. El-Araby; E. K. Shokr, Synthesis, optical linear and non-linear characterization and metal ion sensing application of some novel thieno [2, 3-b] thiophene-2, 5-dicarbohydrazide Schiff base derivatives. *Sci. Rep.* **2025,** *15* (1), 1611.
11. Z S. Zhang, L. Ye and J. Hou, Breaking the 10% efficiency barrier in organic photovoltaics: Morphology and device optimization of well-known PBDTTT polymers. *Adv. Energy Mater.* **2016,** *6* (11), 1502529.
12. E. K. Shokr; M. A. E. Ali; M. S. Kamel; A. El-Araby; A. M. Soliman, Optoelectronic characterizations, and RT-NH3 gas sensing application of newly synthesized spiro [indoline-3, 4′-pyrano [2, 3-b] pyridine] derivative. *Mater. Sci. Semicond. Process* **2025,** *188*, 109201.
13. E. K. Shokr; M. S. Kamel; H. Abdel-Ghany; M. A. E. A. Ali; A. Abdou, Synthesis, characterization, and DFT study of linear and non-linear optical properties of some novel thieno [2, 3-b] thiophene azo dye derivatives. *Mater. Chem. Phys.* **2022,** *290*, 126646.
14. M. O. Aboelez; M. A. E. A. Ali; M.S. Kamel; W. A. Fadaly; M. T. Nemr; H. A. Ezelarab, Novel 3, 4-diaminothieno [2, 3-b] thiophene-2, 5-dicarbohydrazide-based scaffolds as EGFRWT, EGFRT790M, and tubulin polymerization inhibitors with anti-proliferative activity. *Bioorg. Chem.* **2025**, 108728.
15. Y. Wu and W. Zhu, Organic sensitizers from D–π–A to D–A–π–A: effect of the internal electron-withdrawing units on molecular absorption, energy levels and photovoltaic performances. *Chem.Soc. Rev.* **2013,** *42* (5), 2039-2058.

View Article Online
DOI: 10.1039/D6MA00174B

16. L. Jia and Y. Liu, The effects of electron-withdrawing and electron-donating groups on the photophysical properties and ESIPT of salicylideneaniline. *Spectrochim Acta A Mol. Biomol. Spectrosc* **2020,** *242*, 118719.
17. T. Sutradhar and A. Misra, Role of electron-donating and electron-withdrawing groups in tuning the optoelectronic properties of difluoroboron–napthyridine analogues. *J. Phys. Chem. A* **2018,** *122* (16), 4111-4120.
18. Z. Hu, B. Shao, G. T. Geberth and D. A. Vanden Bout, Effects of molecular architecture on morphology and photophysics in conjugated polymers: from single molecules to bulk. *Chem. Sci.* **2018,** *9* (5), 1101-1111.
19. B. J. Schwartz, Conjugated polymers as molecular materials: How chain conformation and film morphology influence energy transfer and interchain interactions. *Annual review of physical chemistry* **2003,** *54* (1), 141-172.
20. Y. Zhou; K. Zhang; Z. Chen; H. Zhang, Molecular design concept for enhancement charge carrier mobility in OFETs: a review. *Mater.* **2023,** *16* (20), 6645.
21. H. F. Haneef, A. M. Zeidell and O. D. Jurchescu, Charge carrier traps in organic semiconductors: a review on the underlying physics and impact on electronic devices. *J. Mater. Chem. C Mater.***2020,** *8* (3), 759-787.
22. A. El-Shafei, A. El-Saghier and E. Ahmed, Synthesis of some new spiro (pyran-4, 2′-benzoxazole) derivatives. *Synthesis* **1994,** *1994* (02), 152-154.
23. M. A. Mohamed, A. M. Kadry, S. A. Bekhit, M. A. Abourehab, K. Amagase, T. M. Ibrahim, A. M. El-Saghier and A. A. Bekhit, Spiro heterocycles bearing piperidine moiety as potential scaffold for antileishmanial activity: synthesis, biological evaluation, and in silico studies. *J Enzyme Inhib Med Chem* **2023,** *38* (1), 330-342.
24. A. H. Abdelmonsef, A. M. El-Saghier and A. M. Kadry, Ultrasound-assisted green synthesis of triazole-based azomethine/thiazolidin-4-one hybrid inhibitors for cancer therapy through targeting dysregulation signatures of some Rab proteins. *Green Chem. Lett. Rev.* **2023,** *16* (1), 2150394.
25. Y. N. Nayak, S. L. Gaonkar and M. Sabu, Chalcones: Versatile intermediates in heterocyclic synthesis. *Journal of Heterocyclic Chemistry* **2023**.
26. M. A. Mohamed, A. M. Kadry, M. M. Farghaly and M. M. El-Saghier, Synthesis, characterization and antibacterial activity of some novel spiro [naphtho [1, 2-e][1, 3] oxazine-3, 4'-pyran] derivatives. *J. Heterocycl. Chem.* **2021,** *7* (3), 1-10.
27. P. Setif, S. Acker, B. Lagoutte and J. Duranton, Contribution to the structural characterization of eucaryotic PSI reaction centre—II. Characterization of a highly purified photoactive SDS-CP1 complex. *Photosynthesis Research* **1980,** *1*, 17-27.
28. E. K. Shokr, S. A. Elkot, M. S. Kamel and H. Ali, Highly efficient (V2O5) 0.91 Zn0. 09 powdered catalyst for water organic pollutant elimination. *Optik* **2024,** *302*, 171718.
29. J R. S. Jassas, O. A. Omran, A. Abdou, M. S. Kamel, Z. Moussa, A. Abd-El-Aziz, N. Ma, H. M. Altass, A. S. Khder and E. M. Hussein, Design and DFT calculations of optoelectronic material based on thiazolobenzimidazole-coupled isatin derivatives. *Mater. Chem. Phys.* **2024,** *325*, 129689.
30. E. K. Shokr, H. Ali, H. A. Mohamed, M. S. Kamel and H. Mohamed, Optical characterization of MoS2 and MoS2/Zn synthesized by thermal evaporation and sol-gel spin-coating techniques for gas-sensing and NLO-applications. *Physica B Condens Matter* **2024,** *683*, 415936.

View Article Online
DOI: 10.1039/D6MA00174B

31. E. K. Shokr, H. A. Mohamed, H. Mohamed, M. S. Kamel and H. Ali, Enhancing the MoS2/MoO3/ZnS/Zn-Heterojunction catalyst's photocatalytic performance for water organic pollutants. *Phys. Scr.* **2023,** *98* (8), 085917.
32. J. Roncali, Molecular bulk heterojunctions: an emerging approach to organic solar cells. *Acc. Chem. Res.* **2009,** *42* (11), 1719-1730.
33. M. Fox, *Optical properties of solids*. Oxford university press: 2010; Vol. 3.
34. F. Urbach, The long-wavelength edge of photographic sensitivity and of the electronic absorption of solids. *Phys. Rev.* **1953,** *92* (5), 1324.
35. M. Sharaf, A. H. Moustafa, M. A. Mohamed, M. S. Kamel, A. Abdou and O. A. Omran, Stereoselective synthesis, optical characterization, DFT, and metal ion detection of tetra p-tert-butylthiacalix [4] arene derivatives containing amide and thiamide fragments at lower rim. *Tetrahedron Let* .**2025,** *168*, 155709.
36. M. Sharaf, A. H. Moustafa, M. A. Mohamed, M. S. Kamel, A. Abdou and O. A. Omran, Optimized design and optical evaluation of mono-chalcone thiacalix [4] arene thin films for UV-blocking and nonlinear photonic applications. *J. Mol. Struct.* **2025**, 144102.
37. T. Moss, A relationship between the refractive index and the infra-red threshold of sensitivity for photoconductors. *J. Chem. Soc.* **1950,** *63* (3), 167.
38. M. A. E. A. A. Ali, M. S. Kamel, S. A. Halim, E. K. Shokr, H. Abdel-Ghany and H. Hamad, Facile synthesis and photodetection characteristics of new pyrrolo [2, 3-b] pyrrole-based metal-free organic dyes containing phenols as the potential candidates towards energy conversion. *Mater. Chem. Phys.* **2023,** *293*, 126972.
39. J. Tauc, R. Grigorovici and A. Vancu, Optical properties and electronic structure of amorphous germanium. *Phys. Status Solidi B.***1966,** *15* (2), 627-637.
40. E. K. Shokr, Optimization of the electrical and optical properties of Sb-Sn-O thin films. *Semicond. Sci. Technol.* **2000,** *15* (3), 247.
41. M. S. Kamel, A. M. Abu Dief, M. A. E. A. A. A. El Remaily, K. A. Abu Al-Ola, A. Y. A. Alzahrani, M. H. AL Mughram and T. N. A. Eskander, Fabrication, Structural Elucidation, and Optical Linear and Nonlinear Characteristics of Ruthenium (III) and Chromium (III) Chelates Generated From Benzylidene-Amino-Phenyl-Phenyl-Methanone Ligand. *ChemistrySelect* **2025,** *10* (36), e02209.
42. E. K. Shokr, S. A. Elkot, M. S. Kamel and H. Ali, Sol-gel spin-coated V2O3 thin films for Optical HCl and Iodine gas sensing. *Opt. Mater.* **2024,** *151*, 115263.
43. A. Mindil, M. S. Kamel, M. Mohery, E. A. Al-Harthi, E. K. Shokr and A. Y. Moustafa, Indium-doped melanin efficient photocatalyst for water purification from organic pollutants. *Phys. Scr.* **2025,** *100* (9), 095523.
44. M. B. Hawsawi, O. A. Omran, A. Abdou, M. S. Kamel, A. M. Almohyawi, M. S. Alluhaibi, R. I. Alsantali, Z. Moussa, A. Timoumi and E. M. Hussein, High nonlinear optical performance of p-tert-butylthiacalix [4] arene derivatives: Synthesis, characterization, and theoretical validation. *Opt. Mater.* **2025,** *160*, 116642.
45. S. Mahjabin, M. M. Haque, S. Khan, V. Selvanathan, M. Jamal, M. Bashar, H. I. Alkhammash, M. I. Hossain, M. Shahiduzzaman and N. Amin, Effects of oxygen concentration variation on the structural and optical properties of reactive sputtered WOx thin film. *Sol. Energy* **2021,** *222*, 202-211.
46. K. Sharma, A. S. Al-Kabbi, G. Saini and S. Tripathi, Determination of dispersive optical constants of nanocrystalline CdSe (nc-CdSe) thin films. *Mater.Res. Bull.* **2012,** *47* (6), 1400-1406.

View Article Online
DOI: 10.1039/D6MA00174B

47. A. Ait Hssi, L. Atourki, N. Labchir, M. Ouafi, K. Abouabassi, A. Elfanaoui, A. Ihlal and K. Bouabid, Optical and dielectric properties of electrochemically deposited p-Cu2O films. *Mater. Res. Express* **2020,** *7* (1), 016424.
48. T. Ghosh, S. K. Sharma and D. Pradhan, Giant Dielectric Constant and Superior Photovoltaic Property of the Mechanochemically Synthesized Stable CH3NH3PbBr3 in a Hole Transporter-Free Solar Cell. *ACS Sustain Chem Eng* **2019,** *8* (3), 1445-1454.
49. W. Steinmann, Optical plasma resonances in solids. *Phys.Status Solidi B.* **1968,** *28* (2), 437-462.
50. S. H. Wemple and M. DiDomenico Jr, Behavior of the electronic dielectric constant in covalent and ionic materials. *Phys. Rev. B* **1971,** *3* (4), 1338.
51. E. K. Shokr, M. S. Kamel, H. Abdel-Ghany and M. A. E. A. A. Ali, Optical characterization and effects of iodine vapor & gaseous HCl adsorption investigation of novel synthesized organic dye based on thieno [2, 3-b] thiophene. *Optik* **2021,** *243*, 167385.
52. J. Tyczkowski and R. Ledzion, Electronic band structure of insulating hydrogenated carbon-germanium films. *J. Appl. Phys.* **1999,** *86* (8), 4412-4418.
53. S. M. Abdelhamid, M. Dongol, A. Elhady and A. A. Abuelwafa, Role of vacuum annealing on the structural, optical properties and Dc conductivity of titanium (IV) phthalocyanine dichloride thin films. *Phys. Scr.* **2023,** *98* (12), 125960.
54. A. A. Abuelwafa, S. Elnobi, M. A. Santos and H. M. Alsoghier, A novel organic semiconductor 4-phenylthiazol-2-yl-(phenylhydrazono) acetonitrile (PTPA) thin films: synthesis, optical and electrical properties. *Scientific Reports* **2023,** *13* (1), 12973.
55. S. I. Qashou, A. Darwish and S. Al Garni, Enhancement of microstructure and electrical conductivity of N, N′-dimethyl-3, 4, 9, 10-perylenedicarboximide nanostructured films by thermal annealing for photoelectronic applications. *Synth. Met.* **2018,** *242*, 67-72.
56. M. El-Nahass, H. Zeyada, K. Abd-El-Rahman and A. A. Darwish, Structural characterization and electrical properties of nanostructured 4-tricyanovinyl-N, N-diethylaniline thin films. *Eur. Phy. J.App. Phys.* **2013,** *62* (1), 10202.
57. G. Chester and A. Thellung, Mott's formula for the thermopower and the Wiedemann-Franz law. *Phys. Rev. B.* **1980,** *21* (10), 4223.
58. G. Chester and A. Thellung, The law of Wiedemann and Franz. *Proc. Phys. Soc.* **1961,** *77* (5), 1005.
59. M. Ibrahim, M. Wakkad and E. K. Shokr, Conduction mechanisms of antimony selenide. *J. Therm. Anal.Calorim* **1994,** *42* (6), 1193-1205.
60. M. Ibrahim, M. Wakkad, E. K. Shokr and H. Abd El-Ghani, Electrical properties of antimony telluride. *Appl .Phys. A.* **1991,** *52* (4), 237-241.
61. Shokr, E. K., Optical properties of glassy Ge20Te80-xSex thin films. *Indian J. Pure Appl. Phys.*. **1992,** *30* (6), 271-275.
62. Q. Wei, M. Mukaida, K. Kirihara, Y. Naitoh and T. Ishida, Recent progress on PEDOT-based thermoelectric materials. *Materials* **2015,** *8* (2), 732-750.
63. J. Ouyang, Q. Xu, C.-W. Chu, Y. Yang, G. Li and J. Shinar, On the mechanism of conductivity enhancement in poly (3, 4-ethylenedioxythiophene): poly (styrene sulfonate) film through solvent treatment. *Polymer* **2004,** *45* (25), 8443-8450.
64. Z. Liang, Y. Zhang, M. Souri, X. Luo, A. M. Boehm, R. Li, Y. Zhang, T. Wang, D.-Y. Kim and J. Mei, Influence of dopant size and electron affinity on the electrical conductivity and thermoelectric properties of a series of conjugated polymers. *J. Mater. Chem. A Mater.* **2018,** *6* (34), 16495-16505.

View Article Online
DOI: 10.1039/D6MA00174B

65. H. Lee, S. B. Lee, Y.-S. Kim, H. Kim, M.-J. Kim, T. W. Yoon, D. Lee, J. H. Cho, Y.-H. Kim and B. Kang, Boosting thermoelectric performance of conjugated polymers via interchain molecular docking: Significance of highly crystalline and percolated morphology. *Chem. Eng. J.* **2023,** *468*, 143654.
66. E. Isotta, B. Mukherjee, C. Fanciulli, N. Ataollahi, I. Sergueev, S. Stankov, R. Edla, N. M. Pugno and P. Scardi, Origin of a simultaneous suppression of thermal conductivity and increase of electrical conductivity and seebeck coefficient in disordered cubic Cu2ZnSnS4. *Phys. Rev. Appl* .**2020,** *14* (6), 064073.
67. N. F. Mott and E. A. Davis, *Electronic processes in non-crystalline materials*. OUP Oxford: 2012.
68. N. K. Hindley, Random phase model of amorphous semiconductors I. Transport and optical properties. *J. Non Cryst. Solids* **1970,** *5* (1), 17-30.
69. F. Benko and F. Koffyberg, Quantum efficiency and optical transitions of CdO photoanodes. *Solid State Commun* .**1986,** *57* (12), 901-903.
70. A. Nozariasbmarz, B. Poudel, W. Li, H. B. Kang, H. Zhu and S. Priya, Bismuth telluride thermoelectrics with 8% module efficiency for waste heat recovery application. *IScience* **2020,** *23* (7).
71. F. Benko and F. Koffyberg, Figure of merit ZT of a thermoelectric device defined from materials properties. *Energy Environ. Sci.* **2017,** *10* (11), 2280-2283.
72. H. Wang, J. H. Hsu, S. I. Yi, S. L. Kim, K. Choi, G. Yang and C. Yu, Thermally driven large n-type voltage responses from hybrids of carbon nanotubes and poly (3, 4-ethylenedioxythiophene) with tetrakis (dimethylamino) ethylene. *Adv. Mater.* **2015,** *27* (43), 6855-6861.
73. G.-H. Kim, L. Shao, K. Zhang and K. P. Pipe, Engineered doping of organic semiconductors for enhanced thermoelectric efficiency. *Nat. Mater.* **2013,** *12* (8), 719-723.
74. Y. Sun, P. Sheng, C. Di, F. Jiao, W. Xu, D. Qiu and D. Zhu, Organic thermoelectric materials and devices based on p-and n-type poly (metal 1, 1, 2, 2-ethenetetrathiolate) s. *Adv. Mater.* **2012,** *24* (7), 932-937.
75. M. Zhang, X. Cao, M. Wen, C. Chen, Q. Wen, Q. Fu and H. Deng,Highly electrical conductive PEDOT: PSS/SWCNT flexible thermoelectric films fabricated by a high-velocity non-solvent turbulent secondary doping approach. *ACS Appl. Mater. Interfaces* **2023,** *15* (8), 10947-10957.
76. N. Wen, Z. Fan, S. Yang, Y. Zhao, T. Cong, S. Xu, H. Zhang, J. Wang, H. Huang and C. Li, Highly conductive, ultra-flexible and continuously processable PEDOT: PSS fibers with high thermoelectric properties for wearable energy harvesting. *Nano Energy* **2020,** *78*, 105361.
77. M. Idir, G. Chamelot, Y. He, T. Lemieux, K. Bueley, S. Beaupré, S. Alem, J. Lu, J.-F. Morin and M. Leclerc, Organic thermoelectric films: achieving high conductivity and power factor through sulfonated-poly (3, 4-ethylenedioxythiophene) and single-walled carbon nanotube composites. *J. Mater. Chem. C Mater.* **2026**.
78. H. Ji, J. G. Lee, H. Lee, D. Kim and K. Cho, High-performance organic thermoelectric materials based on n-type conjugated polymers via chemical isomerization-induced charge transport modulation. *Mater Horiz* **2025,** *12* (21), 9250-9261.

View Article Online
DOI: 10.1039/D6MA00174B

Data Availability Statement

The authors declare that the data supporting the findings of this study are available within the Supplementary file.